AN ABSTRACT OF THE THESIS OF

RICHARD WILLIAM SPINRAD for the degree of MASTER OF SCIENCE
(Name) (Degree)

in OCEANOGRAPHY presented on January 18, 1978
(Major Department) (Date)

Title: EXPERIMENTAL AND THEORETICAL MEASUREMENTS OF THE PARTICULATE VOLUME SCATTERING FUNCTION AT NEAR FORWARD ANGLES.

Redacted for Privacy

Abstract approved:
J. Ronald V. Zaneveld

Narrow angle light scattering measurements were made for various sizes of spherical particles suspended in water. These were compared to calculated theoretical scattering values as derived from the theory of Mie (1908). Through measurements with different particle concentrations at angles between 0.1° and 0.55° the effect of the unscattered main beam light was removed. Results agreed well with Mie theory for these angles. A description of the narrow angle scattering meter is given in detailed form and the working equations are derived.

EXPERIMENTAL AND THEORETICAL MEASUREMENTS OF THE PARTICULATE VOLUME SCATTERING FUNCTION AT NEAR FORWARD ANGLES

by

RICHARD WILLIAM SPINRAD

A THESIS

submitted to
Oregon State University

in partial fulfillment of
the requirements for the
degree of

Master of Science

Completed January 18, 1978

Commencement June 1978

APPROVED:

Redacted for Privacy

Research Associate Professor, Physical Oceanography
in charge of major

Redacted for Privacy

Dean of the School of Oceanography

Redacted for Privacy

Dean of Graduate School

Date thesis is presented January 18, 1978

Typed by Alanna LeCompte for Richard William Spinrad

ACKNOWLEDGMENTS

The method for measuring the narrow angle volume scattering function was suggested as a thesis topic by Dr. J. Ronald V. Zaneveld. The author wishes to thank him for his constant advice and assistance. The author also wishes to congratulate Ron on his tolerance of a graduate student who initially knew very little of optical oceanography.

Appreciation and gratitude is also due Robert Bartz whose knowledge of optical systems proved invaluable in the development and fabrication of a working narrow angle scattering meter.

Moral support was supplied by Ms. Alanna LeCompte and a variety of five string banjos.

This research was supported through funding by the Office of Naval Research contract N00014-76-C-0067 project number NR 083-102

TABLE OF CONTENTS

LIST OF FIGURES

LIST OF TABLES

DEDICATED TO

LEONARD AND THELMA

EXPERIMENTAL AND THEORETICAL MEASUREMENTS OF THE PARTICULATE VOLUME SCATTERING FUNCTION AT NEAR FORWARD ANGLES

I INTRODUCTION

Basic Concepts

The volume scattering function, $\beta(\theta)$, is defined as the radiant intensity, $dI(\theta)$, from a volume element in a given direction, θ, per unit of irradiance, E, incident on the volume and per unit volume, dv, (Jerlov, 1976): $\beta(\theta) = \frac{dI(\theta)}{E dv}$. The measurement of $\beta(\theta)$ of suspended particulate matter in water, especially at very small angles, is a problem which has received considerable attention in the past (Kozlyaninov, 1957; Duntley, 1963; Bauer and Ivanoff, 1965; Morel, 1966; Ochakovsky, 1966; Bauer and Morel, 1967; Morrison, 1967; Kullenberg, 1968; Honey and Sorenson, 1970; Nyfeller, 1970; Brown and Gordon, 1971; Sokolov, et al., 1971; Petzold, 1972; Softley and Dilley, 1972; Wells, et al., 1972; Hodara, 1973; Mertens and Wells, 1973; Morel, 1973a; McCluney, 1974). The importance of small angle measurements lies in the fact that more than half of the scattered radiant intensity is scattered at angles less than 10° from the incident main beam (Kozlyaninov, 1957). In some cases up to 37% of the scattered radiant intensity is scattered within 1° of the incident main beam (Petzold, 1972). It is the particulate content of the water that determines the percent of total scattered radiant intensity within a given angle of the main beam. More specifically, it is the particulate size distribution, indices of refraction and shape distribution that determine this percentage. For this reason the measurement of volume scattering functions at near-forward angles may also be used in conjunction with particle size and shape analysis and scattering measurements at mid-

range angles for the determination of the index of refraction of non-absorbing particles (Zaneveld and Pak, 1973; Zaneveld, et al., 1974). Wells, et al., (1972) have also concluded that small angle scattering deep in the ocean plays a strong role in visibility in sea water. Specifically, the extent of small angle scattering can limit resolution significantly.

A theoretical representation of scattering of electromagnetic waves by spherical, non-absorbing particles was presented by Mie (1908). This theory which is employed for this experiment, indicates that the volume scattering function for a monodisperse system of particles is relatively constant over a range of angles near 0°. The angle at which $\beta(\theta)$ begins to undergo a noticeable decrease varies with particle size, being larger for the smaller particles. Also, at a given angle less than approximately 1°, a larger particle will scatter a greater amount of radiant intensity than a smaller one with the same index of refraction. The theoretical values used in this experiment were obtained from the tables of Salganik and Shifrin (1973). These tables were used because they provided the most values for theoretical scattering at angles less than 1° for a variety of particle sizes. Other references (Chu, et al., 1957; Ashley and Cobb, 1958; Pangonis, et al., 1960; Brown and Gordon, 1971; Morel, 1973b) do not contain as extensive nor as accurate a listing of narrow angle scattering functions.

In this experiment results have been obtained that agree extremely well with the Mie theory values obtained by Salganik and Shifrin (1973). The reason this experiment so successfully substantiates theory is that the effects of the main beam (i.e. unscattered radiant intensity) can

be removed through multiple measurements, as explained in the theoretical discussion of this thesis. Also, the experimental setup was such that the collimation angle of the receiver was limited to approximately one microsteradian by using a very small receiver area.

Survey of previous work

Previous workers have obtained scattering profiles which differed significantly from the theoretical values for small angles ($0°<\theta<1°$). Morrison (1967) used a small angle scattering meter which took readings at approximately 0.2°, 0.6° and 1.2°. The curves obtained of $\beta(\theta)$ vs. θ show a decrease of more than two orders of magnitude in $\beta(\theta)$ from $\theta = 0.1°$ to $\theta = 1°$ ($\beta(\theta)$ for $\theta<0.2°$ was interpolated in his curves). Morrison's experimental setup was such that large amounts of unscattered main beam radiant intensity were detected by the receiver. In addition, with measurements at 0.2° and 0.6° Morrison had to interpolate values of $\beta(\theta)$ between these two angular values and at all angles less than 0.2°. The resultant interpolation indicated a very large slope in $\beta(\theta)$ vs. θ at angles less than 1°.

Wells, et al., (1972) measured a point spread function and got results similar to those of Morrison for much the same reason. The point spread function is defined as the apparent or virtual distribution of luminous intensity from a point source viewed through the scattering medium (Wells, et al., 1972). Hodara (1973) describes indirect measurements of $\beta(\theta)$ through modulation transfer function (MTF) measurements. A scattered "blur circle" from a beam source is projected through a series of slits logarithmically decreasing in width. Next, a Fourier analysis is performed on the blur circle. The volume scattering function is then extracted through manipulation of a modulation transfer function obtained from the Fourier analysis. The results Hodara obtained with an MTF meter agreed well with theoretical results at angles greater than 2°. At small angles the values obtained

were much larger than theory predicts. In all of the experiments just described the causes for the discrepancy between theory and experiment are lack of beam collimation, inclusion of main beam intensity and/or insufficient data points at angles less then 1°. Honey and Sorenson (1970) concluded that turbulent fluctuations in the refractive index of water would contribute significantly to scattering only at angles less than 0.004°. The experiment described herein was performed in a much larger angular region, so scattering induced by turbulence could be ignored.

II SCATTERING THEORY

Mie Theory for Narrow Angle Scattering

In 1908, Mie, using the equations and laws of electromagnetic theory, derived a series of expressions to describe the perturbation of a plane monochromatic electromagnetic wave by spherical non-absorbing particles. The assumptions made in Mie theory are that the scattered light has the same wavelength as the incident light and that the particles are independent. Independence implies that the scattering properties of one particle will not affect the scattering properties of any other particle. That is, interference of scattered electromagnetic waves is random. Van de Hulst (1957) later stated that independence also requires that the distance between spheres be greater than or equal to three times their radii.

An excellent description of Mie theory and the derivation thereof can be found in Roach (1974). The complete mathematical description of the theory is lengthy and not essential to the body of this thesis. The results of the derivation are important, however.

If an incident randomly polarized beam of radiant intensity is scattered in a direction θ, the scattered radiant intensity may be divided into a quantity of intensity whose electric vector, i_1, is perpendicular to the plane of observation, and a quantity of intensity whose electric vector, i_2, is parallel to the plane of observation. Mie theory provides the following expressions for i_1 and i_2:

$$i_1 = \left(\sum_{n=1}^{\infty} \left(A_n \frac{dP_n(x)}{dx} + B_n \left| x \frac{dP_n(x)}{dx} - (1-x^2) \frac{d^2P_n(x)}{dx^2} \right| \right) \right)^2 \qquad (1)$$

$$i_2 = \left(\sum_{n=1}^{\infty} \left(A_n \left| x \frac{dP_n(x)}{dx} - (1 - x^2) \frac{d^2P_n(x)}{dx^2} \right| + B_n \frac{dP_n(x)}{dx} \right) \right)^2 \qquad (2)$$

Where $x = - \cos \theta$

$P_n(x)$ = Legendre polynomial of order n

A_n and B_n are functions involving Riccati-Bessel and Riccati-Hankel functions.

The values of i_1 and i_2 depend only upon the angle θ, the particle diameter, D, the wavelength of the incident beam, λ, and the refractive index, m, of the particle relative to that of water in this case. From these expressions, the volume scattering function for one particle per unit volume is given by

$$i(\theta) = \frac{\lambda^2}{8\pi^2} (i_1 + i_2) \qquad (3)$$

or

$$\beta(\theta) = Ni(\theta) \qquad (4)$$

Where N = the number of particles per unit volume.

Salganik and Shifrin (1973) have calculated the values of $i_1 + i_2$ for values of $\theta = 0°$, $0.2°$, $0.5°$ and $1°$; D = 0.06 μm to 40 μm; m = 1.02, and 1.15 for concentrations of one particle per m^3. Figures 1 through 5 show the theoretical values of $i(\theta)$ vs. θ for five different particle diameters with relative indices of refraction of 1.02 and 1.15 at small angles. Figures 6 through 10 show the theoretical values of $i(\theta)$ vs. θ for five different particle diameters with relative indices of refraction

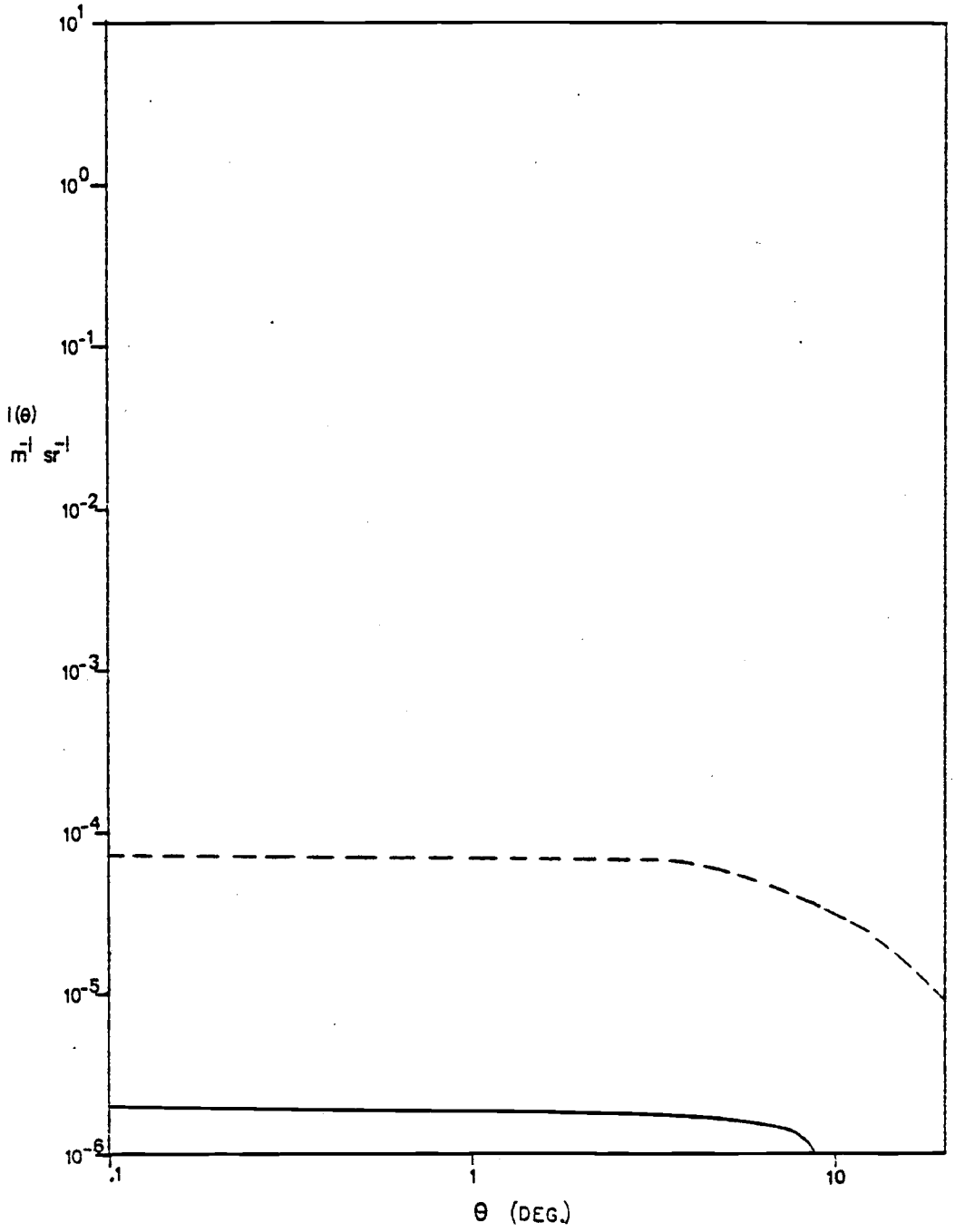

Fig. 1. Theoretical volume scattering function of 2.01 μm diameter particles at small angles for relative indices of refraction of 1.02 (solid line) and 1.15 (dotted line).

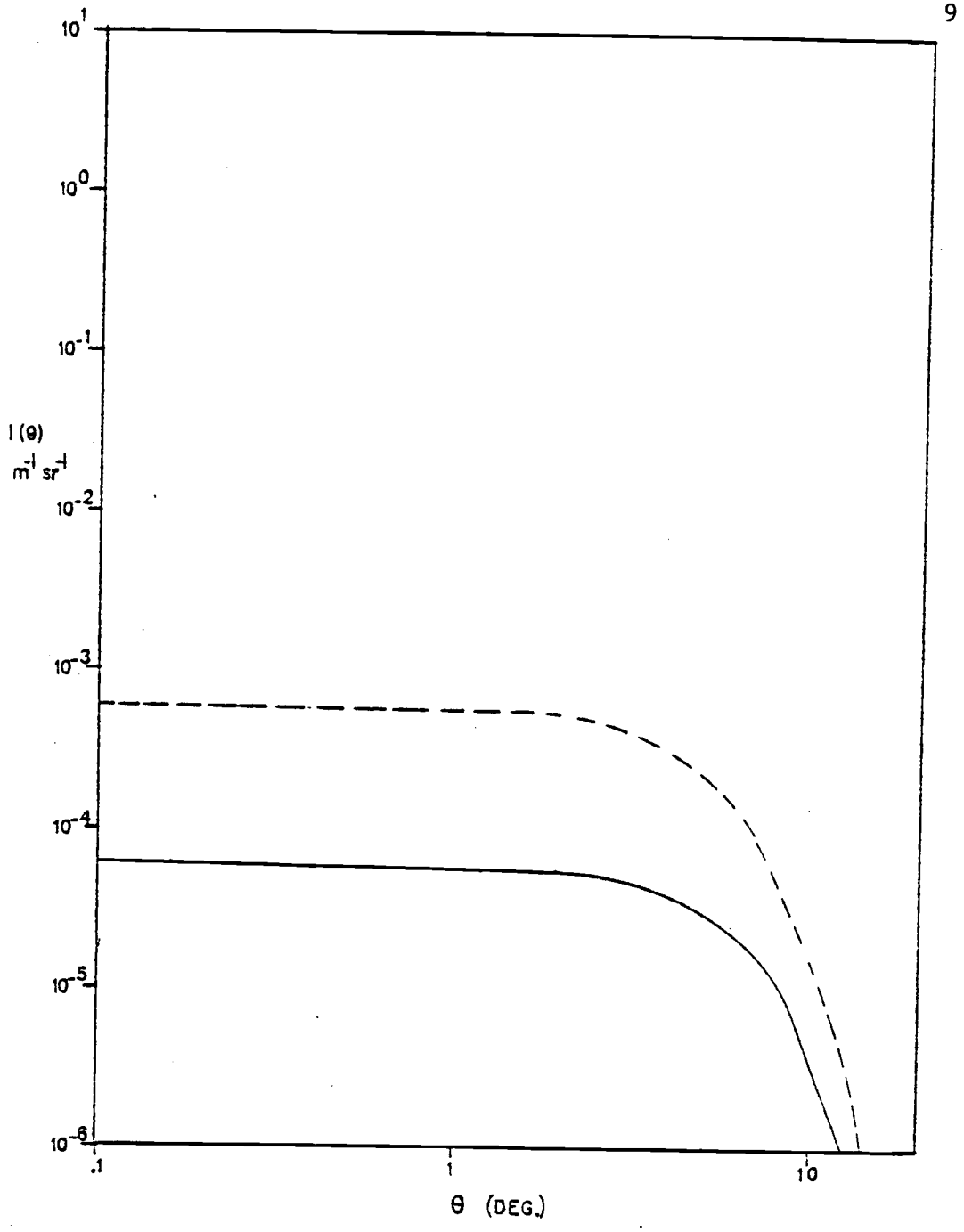

Fig. 2. Theoretical volume scattering function of 3.63 μm diameter particles at small angles for relative indices of refraction of 1.02 (solid line) and 1.15 (dotted line).

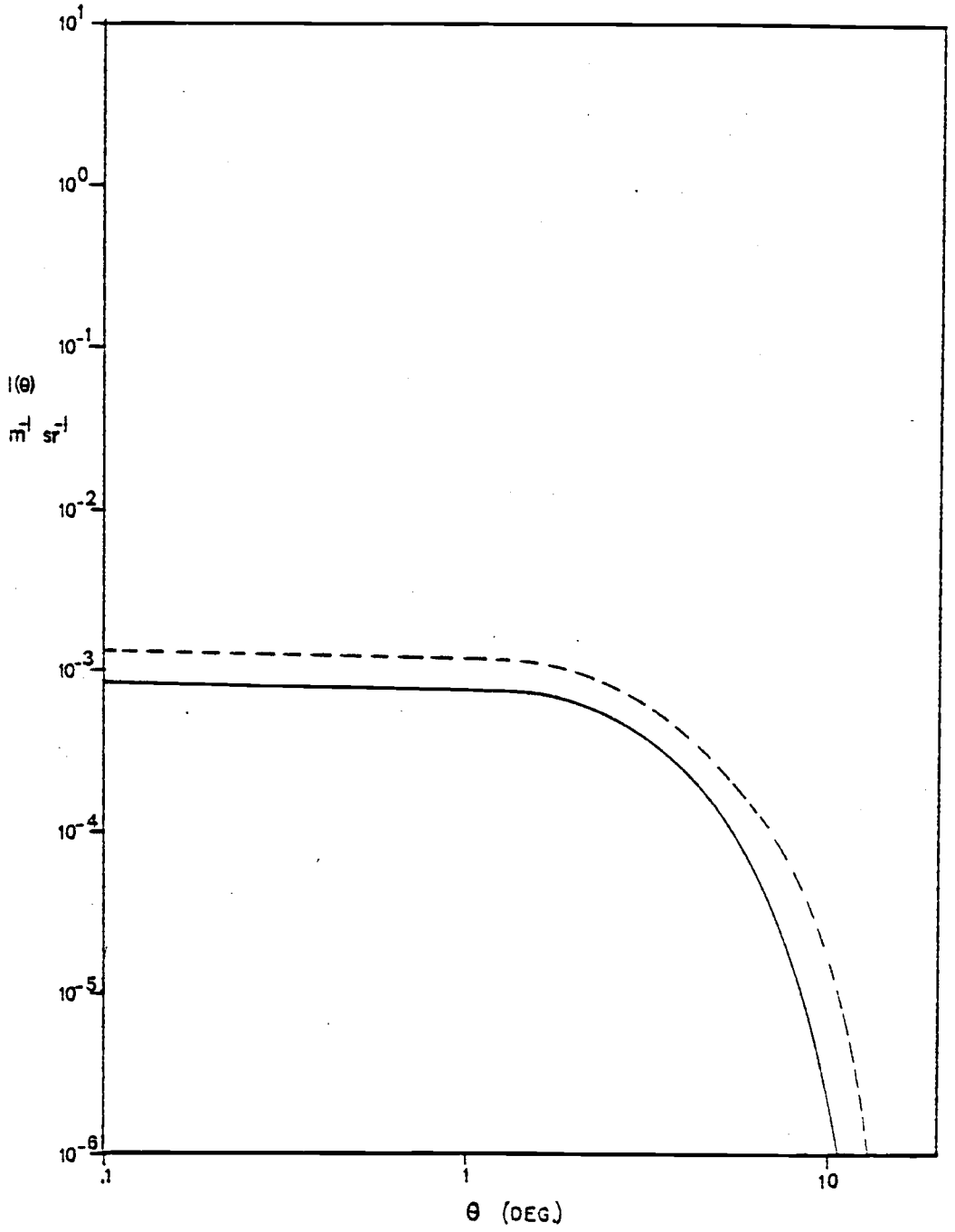

Fig. 3. Theoretical volume scattering function of 5.64 μm diameter particles at small angles for relative indices of refraction of 1.02 (solid line) and 1.15 (dotted line).

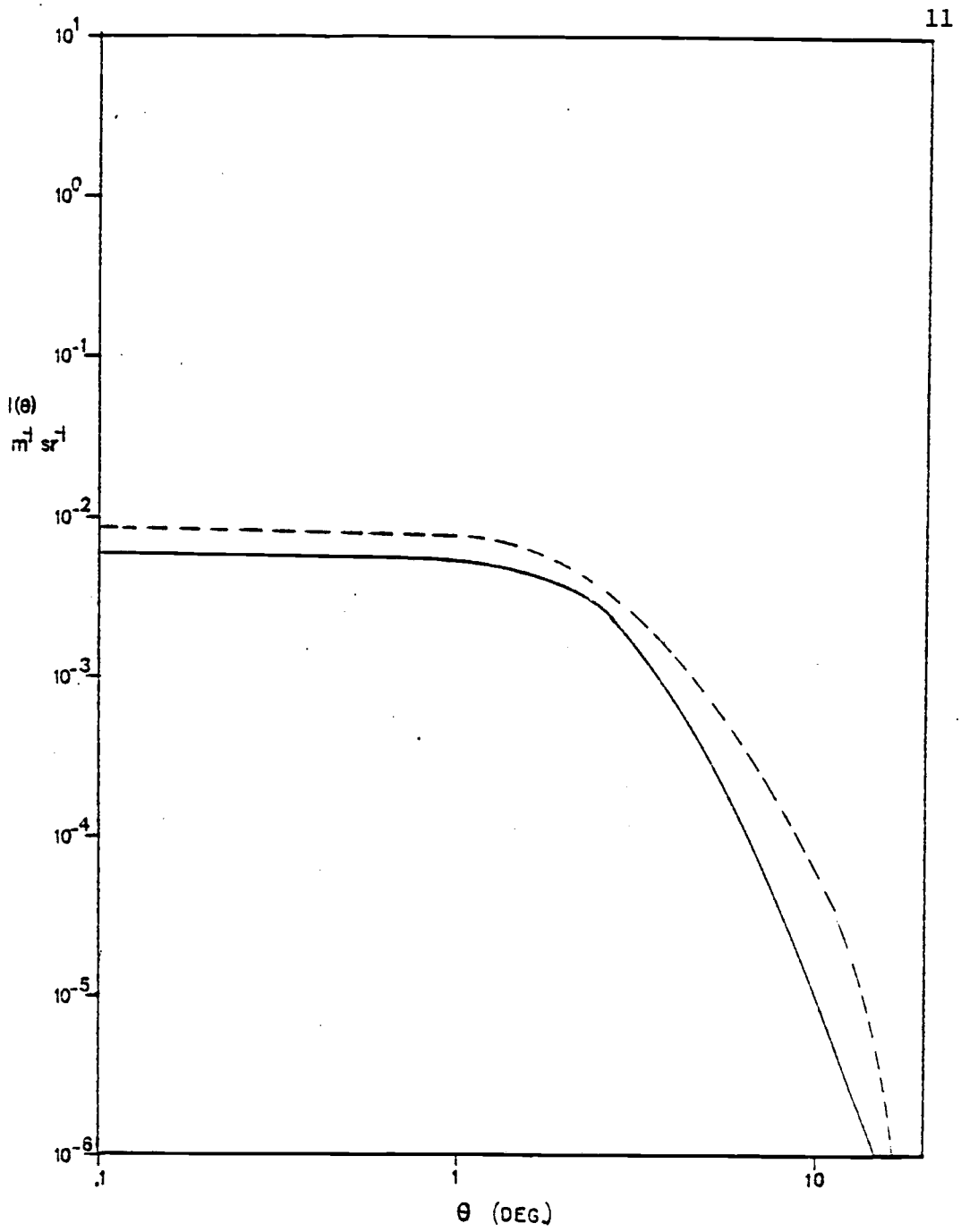

Fig. 4. Theoretical volume scattering function of 8.06 μm diameter particles at small angles for relative indices of refraction of 1.02 (solid line) and 1.15 (dotted line).

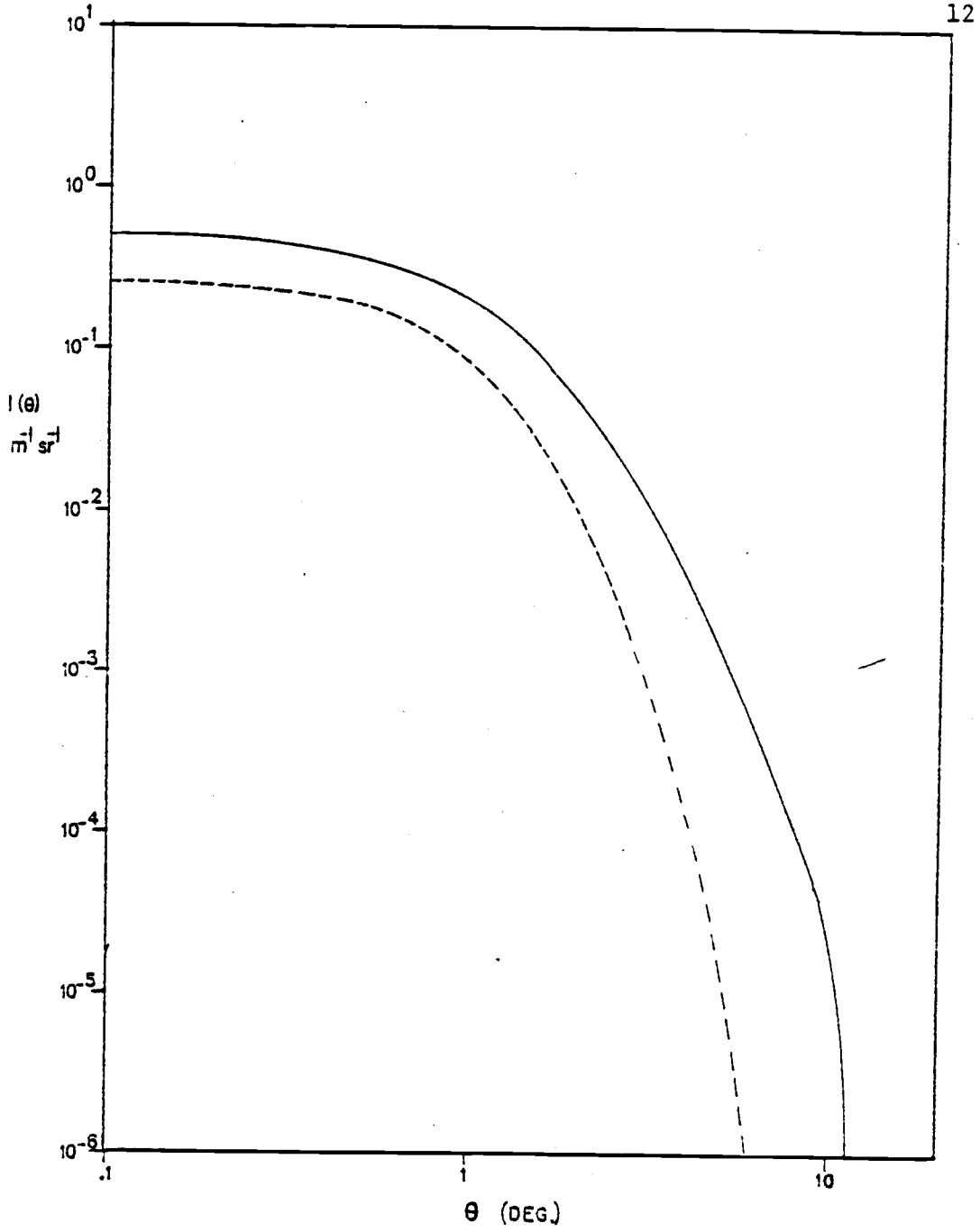

Fig. 5. Theoretical volume scattering function of 19.34 μm diameter particles at small angles for relative indices of refraction of 1.02 (solid line) and 1.15 (dotted line.)

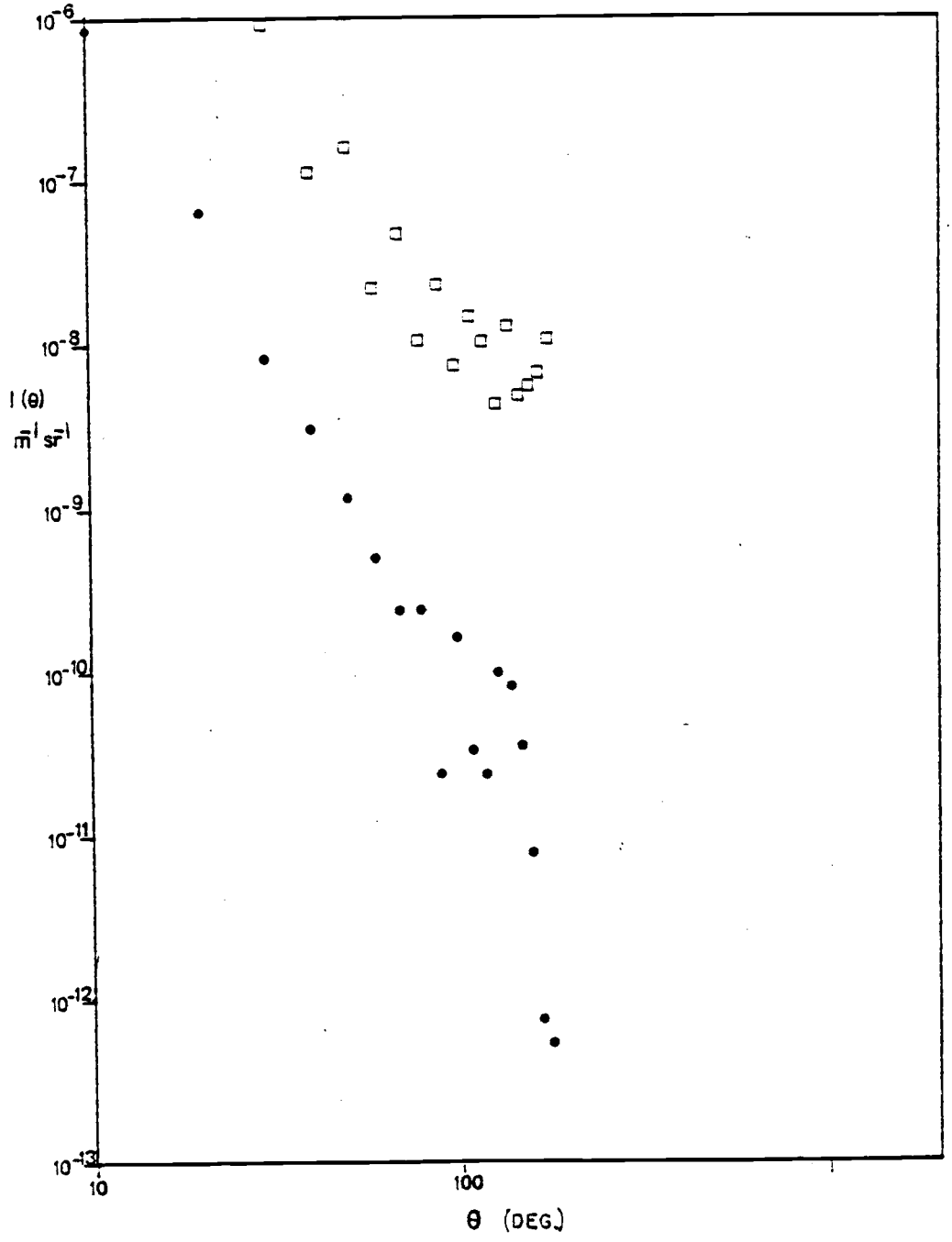

Fig. 6. Theoretical volume scattering function of 2.01 μm diameter particles at mid-range and large angles for relative indices of refraction of 1.02 (circles) and 1.15 (squares).

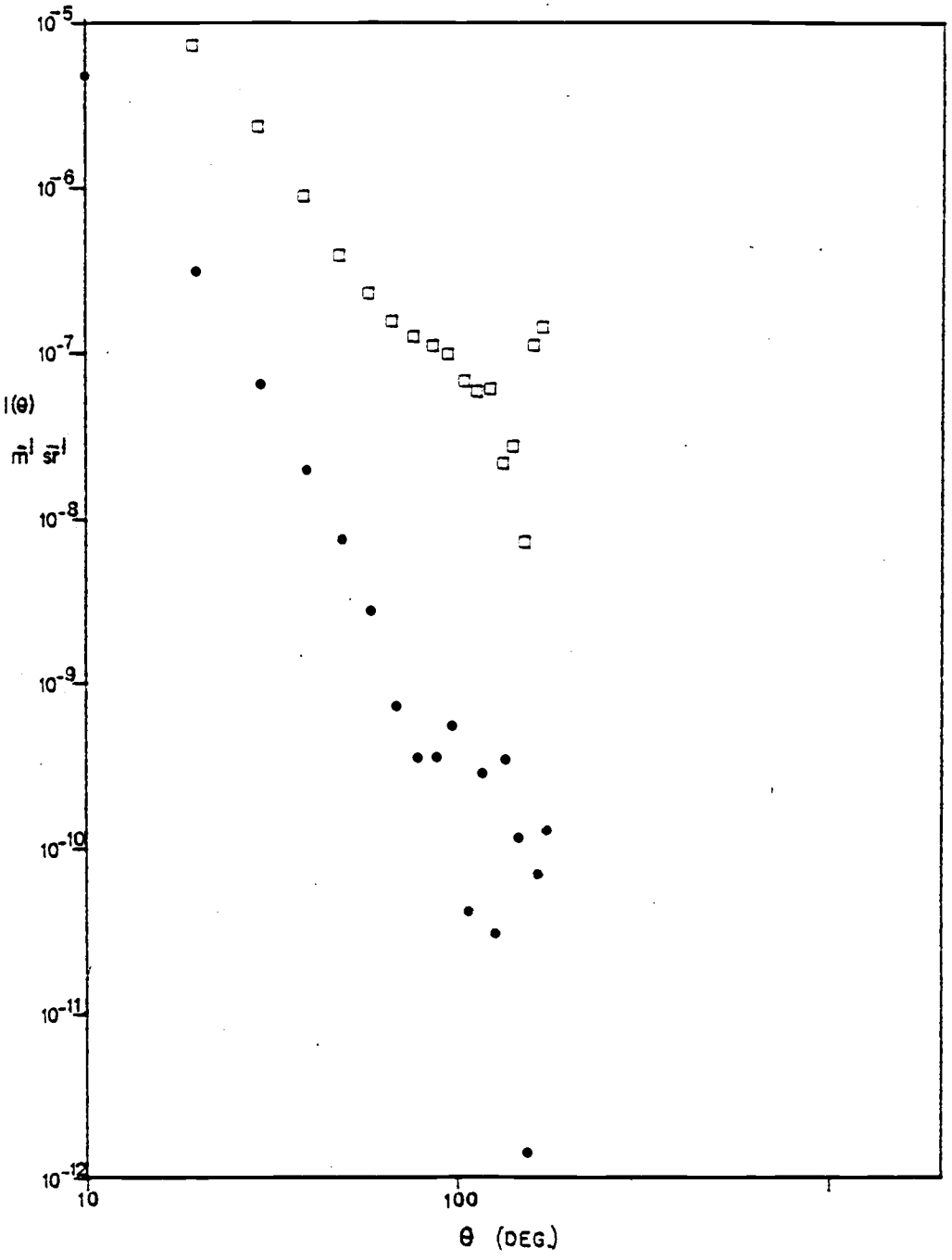

Fig. 7. Theoretical volume scattering function of 3.63 μm diameter particles at mid-range and large angles for relative indices of refraction of 1.02 (circles) and 1.15 (squares).

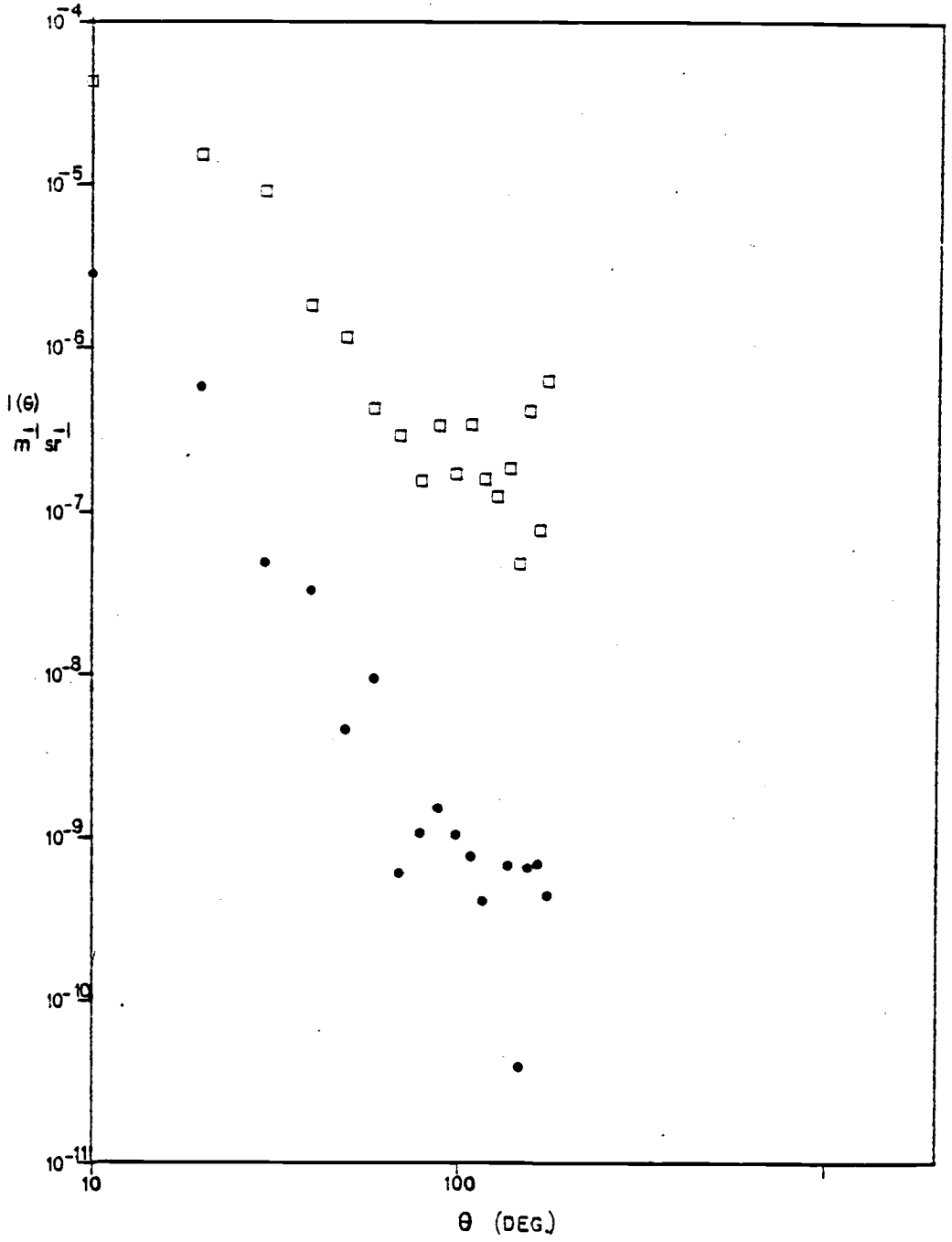

Fig. 8. Theoretical volume scattering function of 5.64 μm diameter particles at mid-range and large angles for relative indices of refraction of 1.02 (circles) and 1.15 (squares).

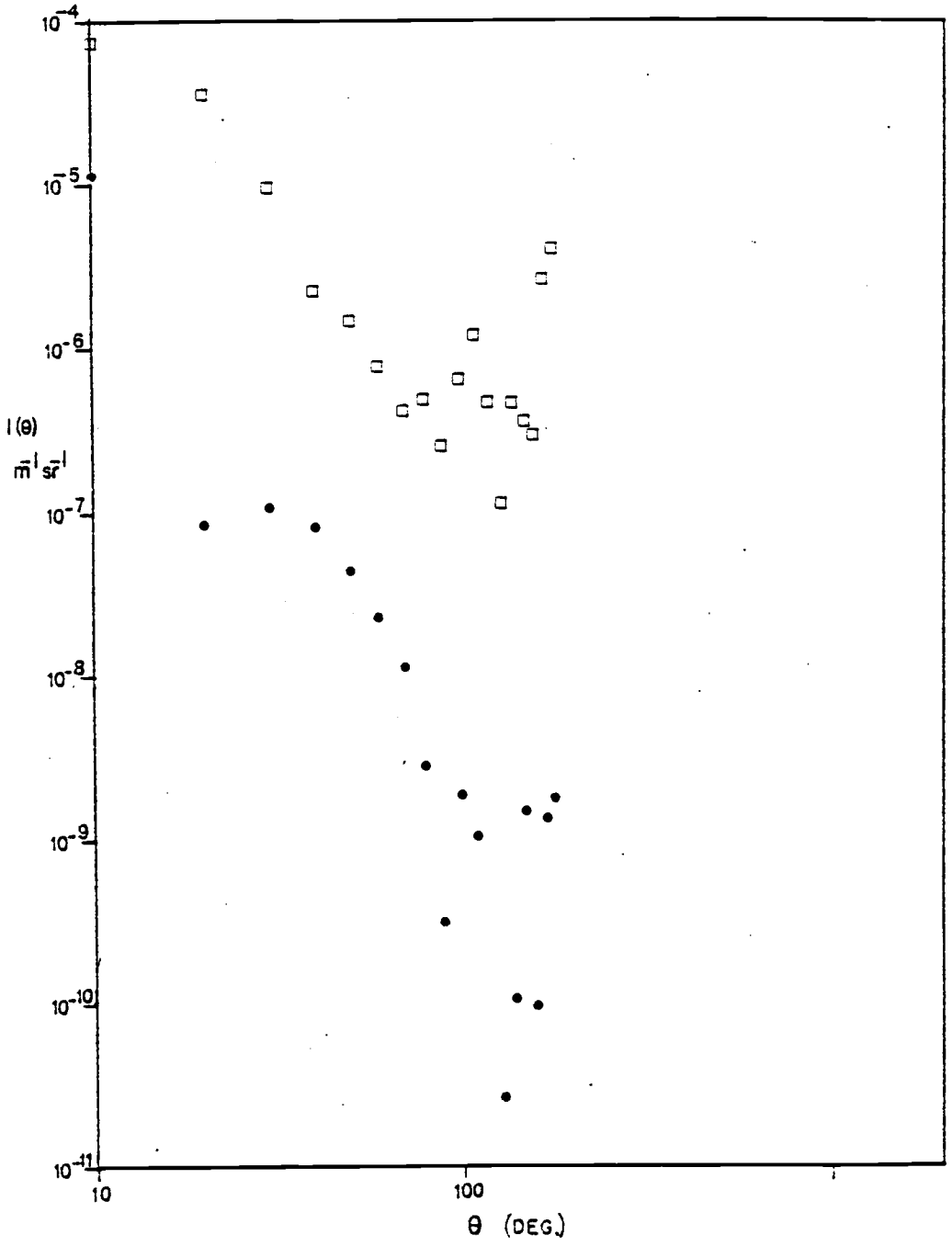

Fig. 9. Theoretical volume scattering function of 8.06 μm diameter particles at mid-range and large angles for relative indices of refraction of 1.02 (circles) and 1.15 (squares).

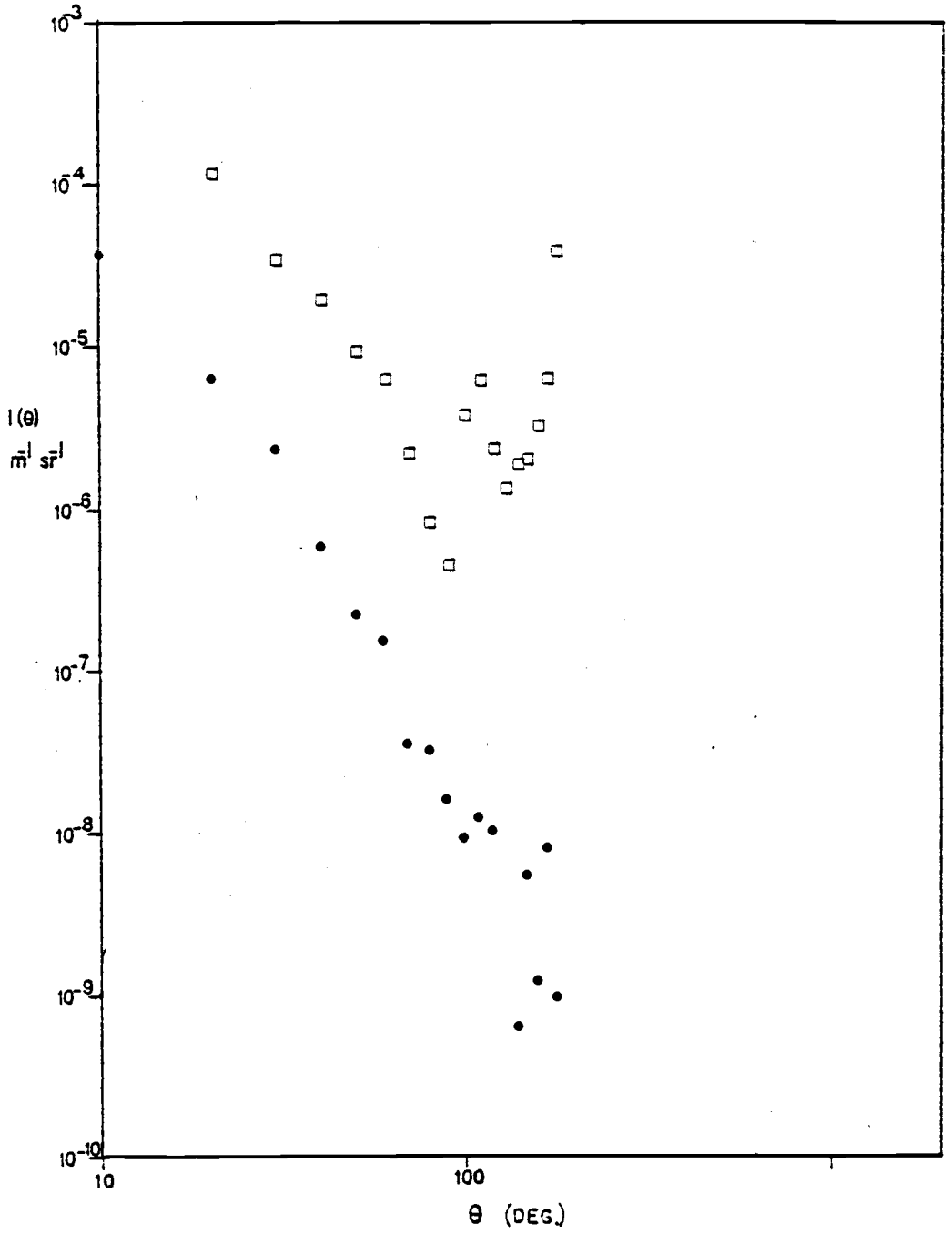

Fig. 10. Theoretical volume scattering function of 19.34 μm diameter particles at mid-range and large angles for relative indices of refraction of 1.02 (circles) and 1.15 (squares).

of 1.02 and 1.15 for mid-range and large scattering angles. Figure 11 shows the value of $\beta(\theta)$ vs. θ for a distribution composed of one particle per ml each of five particle sizes. Similarly, for a given particle size distribution a Mie scattering curve may be obtained.

In Figures 12 and 13 the theoretical volume scattering functions of a Junge (1963) type distribution of particles is shown for various particulate indices of refraction at small and large angles respectively. The Junge distribution used is given by $f(a) = a^{-5.0}$ where a is the particle radius and f(a) is the number of particles per unit volume having a radius larger than a. The range of particle diameters, 2a, used for these figures is 0.06 μm to 40.28 μm. Figure 14 shows a comparison of the theoretical values of the volume scattering function for the same Junge distribution at various indices of refraction as computed by Morel (1973a) and Salganik and Shifrin (1973). This figure shows the variability of numerical analysis for theoretical calculations of the volume scattering functions. Experimental results cannot be verified within any greater accuracy than this variability allows.

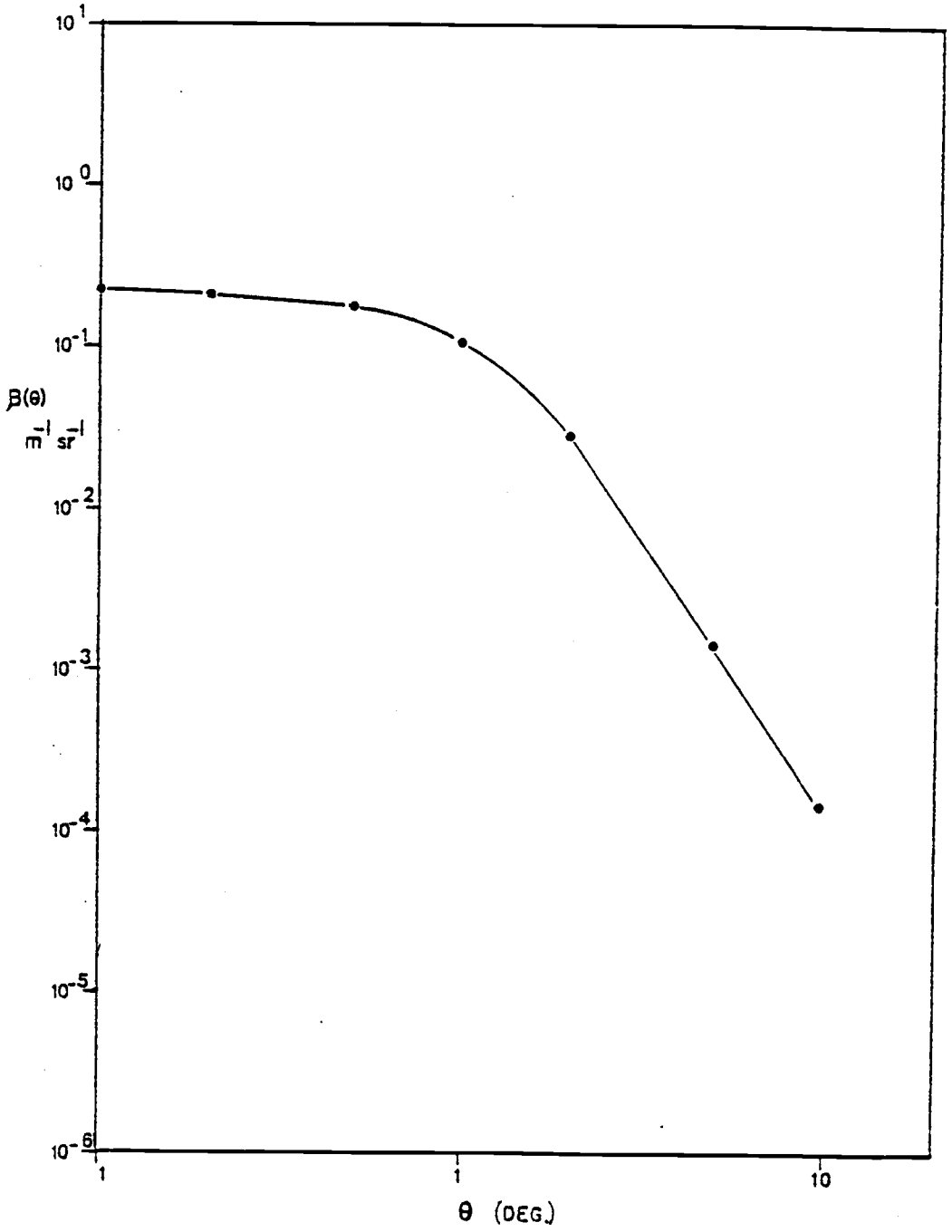

Fig. 11. Theoretical volume scattering function for one particle per ml of each size: 2.01 μm, 3.63 μm, 5.64 μm, 8.06 μm, 19.34 μm, relative index of refraction is 1.15.

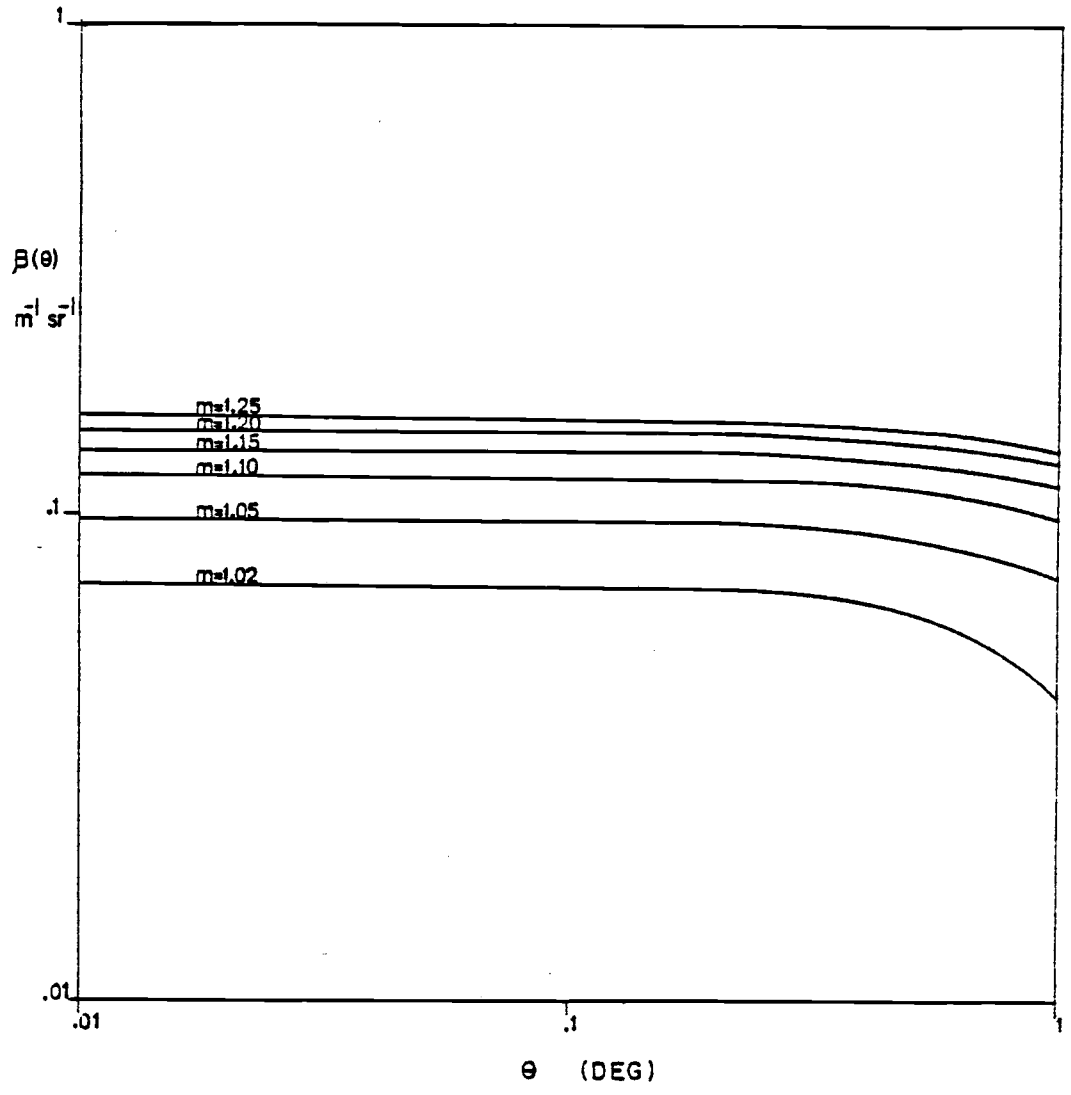

Fig. 12. Volume scattering function of Junge-type distribution of particles at small angles for various relative indices of refraction. Junge exponent = 5.0.

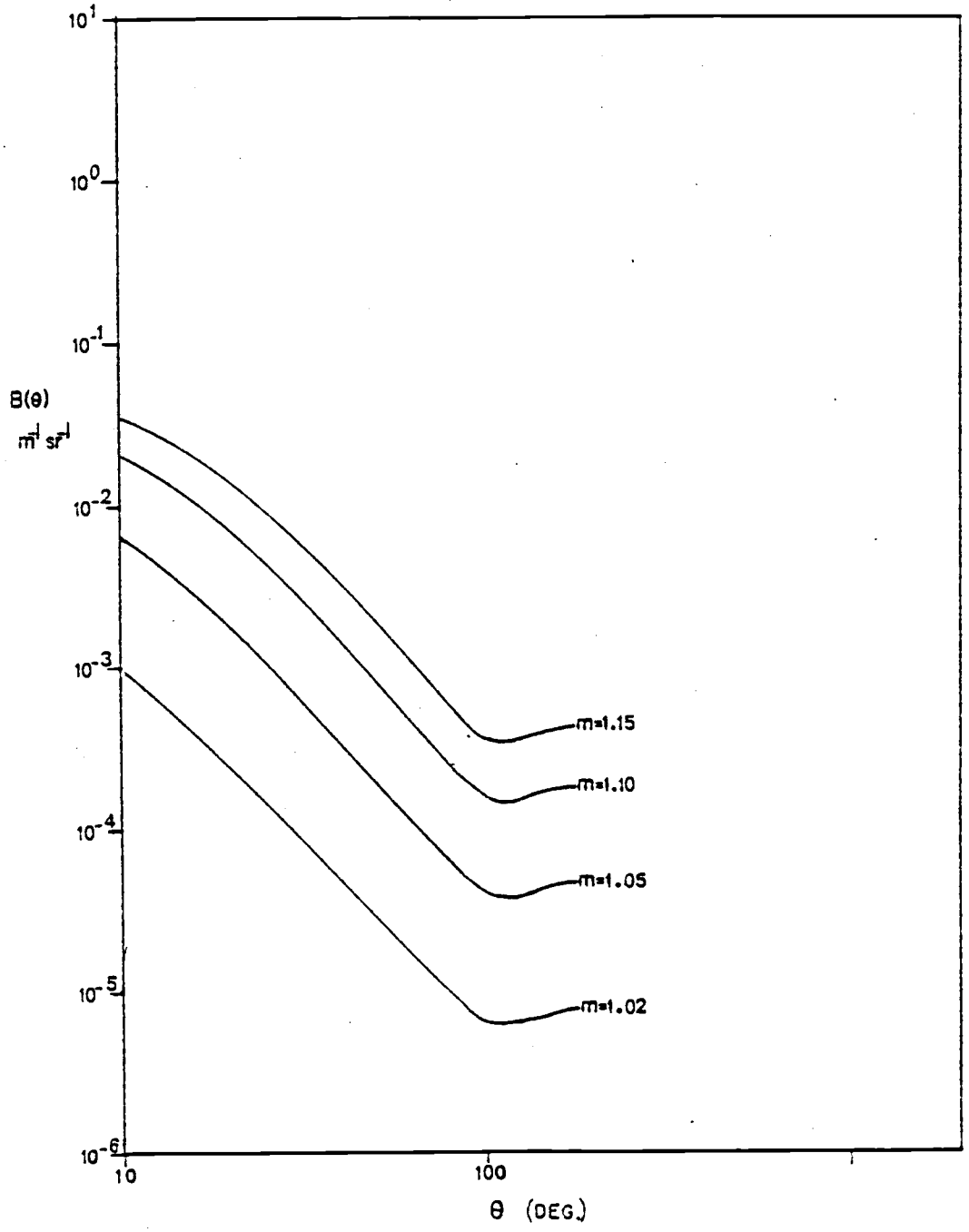

Fig. 13 Volume scattering function of Junge-type distribution of particles at mid-range and large angles for various relative indices of refraction. Junge exponent = 5.0.

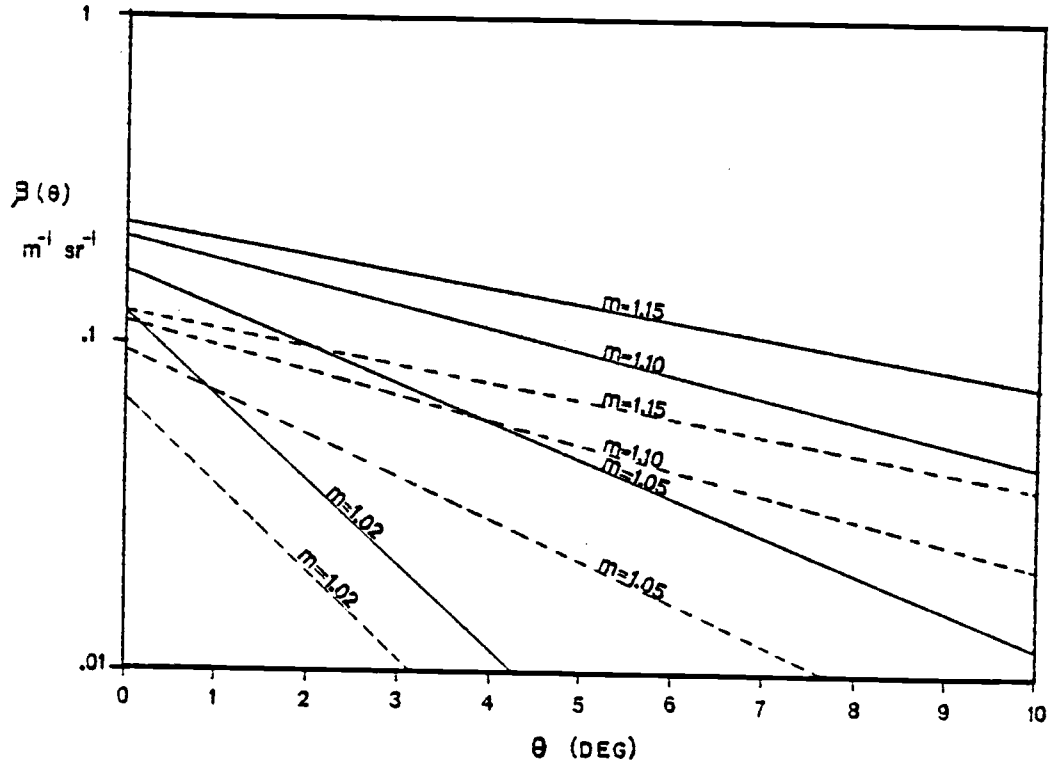

Fig. 14 A comparison of the theoretical volume scattering function calculations of Morel (1973b; solid line) and Salganik and Shifrin (1973; dotted line) for a Junge-type distribution of particles at mid-range angles for various relative indices of refraction. Junge exponent = 5.0.

Derivation of working equations for $\beta(\theta)$

Attenuation of light in the sea is due only to absorption and scattering caused by the sea water and any particles or substances contained in the sea water. Specifically:

$$c = a + b \qquad \text{(after Jerlov, 1976)}$$

Where c = the attenuation coefficient defined as the attenuation of an infinitesimally thin layer of the medium normal to the beam of light, divided by the thickness of the layer. (In units of m^{-1})

a = the absorption coefficient defined as the absorption of an infinitesimally thin layer of the medium normal to the beam of light, divided by the thickness of the layer. (In units of m^{-1})

b = the scattering coefficient defined as the scattering of an infinitesimally thin layer of the medium normal to the beam of light, divided by the thickness of the layer. (In units of m^{-1})

The total scattering coefficient, b, is related to the volume scattering function, $\beta(\theta)$, as follows:

$$b = 2\pi \int_0^{\pi} \beta(\theta) \sin \theta \, d\theta \qquad (6)$$

where θ = the angle relative to the direction of the main beam.

In addition, $\beta(\theta)$ may be defined as follows:

$$\beta(\theta) = \frac{dI(\theta)}{E \, dv} \qquad \text{(Jerlov, 1976)} \qquad (7)$$

where $dI(\theta)$ = scattered radiant intensity at angle θ (watts/steradian)

E = incident irradiance (watts/m^2)

dv = volume element from which $dI(\theta)$ is scattered (m^3)

In any small angle optical measurement the appearance of unscattered light from the finite main beam must be considered. In addition, it must be realistically assumed that the direct light is not perfectly collimated and that there may be some scattering from the lenses in the optical setup. Therefore, the power received at a detector, P_r, when not aimed directly at the light source, will be equal to the power received due to scattering, P_β, plus the "noise", P_n, due to main beam inclusion, lack of collimation, and scattering from the lenses; specifically if a detector of small area is placed at an angle, θ from the main beam, the power it receives is given by:

$$P_r(\theta) = P_\beta(\theta) + P_n(\theta) \tag{8}$$

Consider Figure 15, which shows an elementary scattering volume spaced on the center line of the apparatus:

$$dI(\theta) = \frac{dP_\beta(\theta) e^{c(L - x)}}{\omega_\theta} \tag{9}$$

where $dP_\beta(\theta)$ = power received due to scattering from the volume element, dv.

The irradiance on the volume element dv is:

$$E = \frac{P_o e^{-cx}}{A} \tag{10}$$

where P_o is the incident power in watts

with the volume element dv defined as:

$$dv = Adx \tag{11}$$

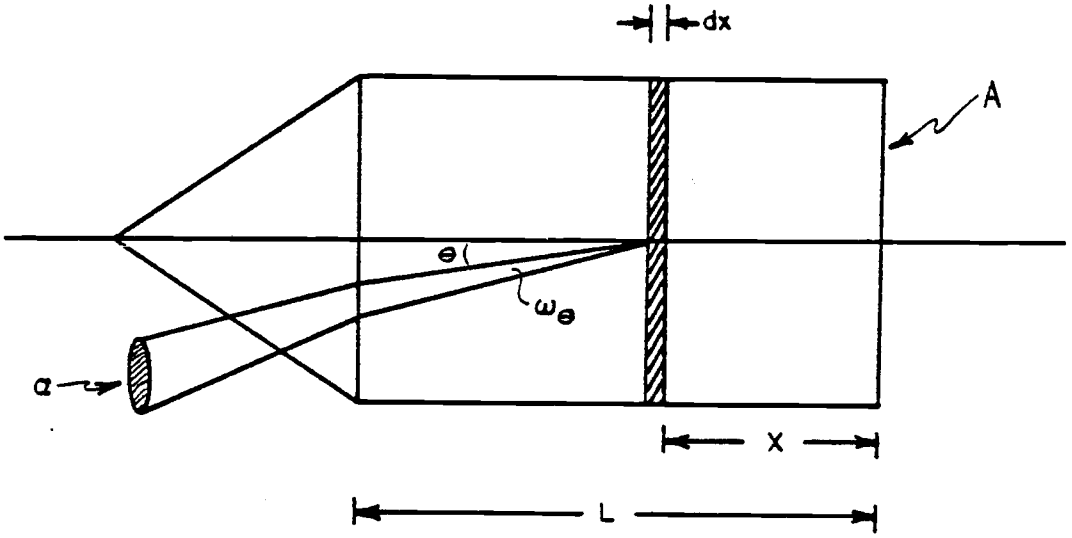

Fig. 15 An elementary scattering volume as viewed normal to the plane of incidence.

equation (7) now becomes

$$\beta(\theta) = \frac{dP_\beta(\theta) e^{c(L - x)}}{\omega_\theta \frac{P_o e^{-cx}}{A} A dx}$$

or $$dP_\beta(\theta) = \beta(\theta)\omega_\theta P_o e^{-cL} dx \qquad (13)$$

Integration of $dP_\beta(\theta)$ over the length of the cell yields the total power received due to scattering by particulate matter and water:

$$P_\beta(\theta) = \int_o^L dP_\beta(\theta) = \beta(\theta)\omega_\theta P_o L e^{-cL} \qquad (14)$$

Total power received can therefore be expressed as:

$$P_r(\theta) = P_n(\theta) + \beta(\theta)\omega_\theta P_o L e^{-cL} \qquad (15)$$

Furthermore, the scattering function, $\beta(\theta)$ can be divided into scattering due to particles $\beta_p(\theta)$, and scattering due to water $\beta_w(\theta)$:

$$\beta(\theta) = \beta_p(\theta) + \beta_w(\theta) \qquad (16)$$

$$P_r(\theta) = P_n(\theta) + \left[\beta_p(\theta) + \beta_w(\theta)\right] \omega_\theta P_o L e^{-cL} \qquad (17)$$

If the particle concentration is increased by a factor, F, then the particle scattering function will also increase by a factor, F. That is, scattering is additive provided multiple scattering does not occur (the cell volume and the particle concentrations were such that multiple scattering was not considered in this experiment). The scattering due to the water alone remains constant, of course.

$$P_{r_1}(\theta) = P_{n_1}(\theta) + \left[\beta_p(\theta) + \beta_w(\theta)\right] \omega_\theta P_o e^{-c_1 L} L \qquad (18)$$

$$P_{r_2}(\theta) = P_{n_2}(\theta) + \left[F\beta_p(\theta) + \beta_w(\theta)\right] \omega_\theta P_o e^{-c_2 L} L \qquad (19)$$

The noise received during the first measurement will be reduced with the addition of particles. This reduction is equal to the ratios of the transmissivities:

$$T_1 = e^{-c_1 L} = \frac{P_{r_1}(o)}{P_o} \tag{20}$$

$$T_2 = e^{-c_2 L} = \frac{P_{r_2}(o)}{P_o} \tag{21}$$

$$P_{n_2}(\theta) = P_{n_1}(\theta) \frac{T_2}{T_1} = P_{n_1}(\theta) \frac{e^{-c_2 L}}{e^{-c_1 L}} = P_{n_1}(\theta)\, e^{-(c_2 - c_1)L} \tag{22}$$

Therefore, equation (15) becomes:

$$P_{r_2}(\theta) = P_{n_1}(\theta) e^{-(c_2-c_1)L} + \left\{ F\beta_p(\theta) + \beta_w(\theta) \right\} \omega_\theta\, P_o\, e^{-c_2 L} L \tag{23}$$

Multiplying equation (18) by $e^{-(c_2-c_1)L}$ and subtracting equation (19) yields:

$$P_{r_1}(\theta)\, e^{-(c_2-c_1)L} - P_{r_2}(\theta) = \left\{ \beta_p(\theta) + \beta_w(\theta) \right\} \omega_\theta\, P_o\, e^{-c_2 L} L - \left\{ F\beta_p(\theta) + \beta_w(\theta) \right\} \omega_\theta\, P_o\, e^{-c_2 L} L \tag{24}$$

$$= (1-F)\beta_p(\theta)\omega_\theta\, P_o\, e^{-c_2 L} L \tag{25}$$

$$\beta_p(\theta) = \frac{P_{r_1}(\theta) e^{c_1 L} - P_{r_2}(\theta) e^{c_2 L}}{(1-F)\, \omega_\theta\, P_o\, L} \tag{26}$$

Using the transmissivities as defined in equations (20) and (21), equation (26) can be simplified as:

$$\beta_p(\theta) = \frac{\dfrac{P_{r_1}(\theta)}{P_{r_1}(o)} - \dfrac{P_{r_2}(\theta)}{P_{r_2}(o)}}{(1-F)\, \omega_\theta\, L} \tag{27}$$

Thus, with two measurements at different particle concentrations, the particle scattering function can be calculated.

III EXPERIMENTAL SETUP

General Description

The setup for the small angle experiment basically consists of two systems: a particle size analyzer and a narrow angle scattering meter. In order to compare experimental values of narrow angle scattering with theoretical values it is necessary to know what the exact particle size distribution of a given sample is. The tables of theoretical scattering values which are used (Salganik and Shifrin, 1973) are designed such that theoretical volume scattering functions can only be calculated if the sample particle size distribution is know.

The particle size analyzer is composed of Coulter Counter glassware and a Nuclear Data pulse height analyzer. In this experiment the particles used are of three mean diameters: 5.2 μm, 8 μm and 9.8 μm.

The narrow angle scattering meter is essentially a light source, a cell with water and particles through which the light passes, and a receiver positioned at the exact location where scattered light is to be detected. Each of the individual components of the meter will be described in detail herein.

Components of Narrow Angle Scattering Meter

A schematic drawing of the narrow angle scattering meter is shown in Figure 16.

A. Laser

The laser used in this experiment is a University Laboratories model number 1H361 helium-neon laser emitting randomly polarized light at 632.8 nanometers wavelength. The power of the beam emitted is two milliwatts and the laser operates off a regulated power supply. The laser is mounted with posts on an adjustable rail to facilitate aligning the beam.

B. Lens and pinhole combination

The lens and pinhole combination is used to approximate a point source of light. This allows for better collimation of the beam within the scattering cell. The lens is a plano-convex lens with a focal length of 80 mm. It is placed directly in front of the laser. The pinhole, which is 1.0 mm in diameter, is placed at the focal point of the lens to filter out any uncollimated light, or reflections off the lens. Light from the laser which is not collimated will therefore not be focused through the pinhole so the lens and pinhole combination can act as an effective collimator.

C. Cylindrical scattering cell

The cylindrical scattering cell is a pyrex open-ended cylinder with a length of 0.5 meters and with a diameter of 8.85 cm. It has three open nipples to allow for filling or emptying of the cell or for in-line filtrations. A plano-convex lens of focal length 1.0 m

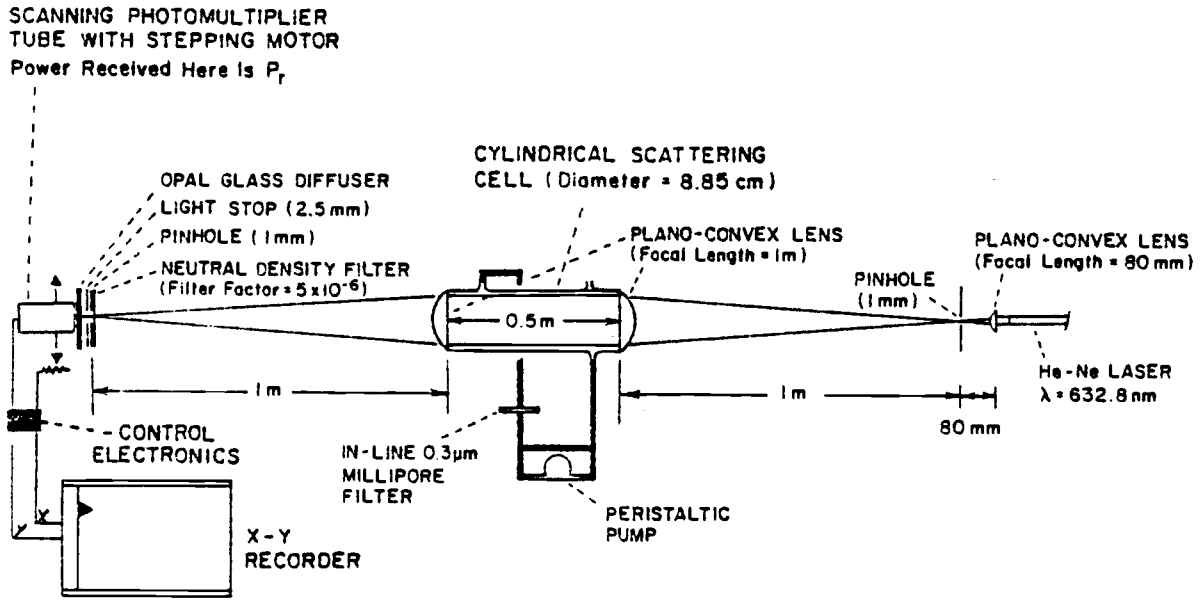

Fig. 16. Schematic drawing of the laboratory setup of the small angle scattering meter.

is placed on each end of the tube and secured to prevent water leakage. The lens on the right side of the cell is placed exactly 1.0 m from the pinhole described above. The lens on the left side is placed exactly 1.0 m from the detector unit.

D. Pumping and filtration system

In order to remove the particles from the water in the cell after one experiment and before the next it is necessary to continually filter the water until all the particles have been removed. Tygon tubing is used to connect the lower nipple on the cylindrical scattering cell to the peristaltic pump which is driven by a small electric motor. After the pump the tubing continues up to an in-line filtering apparatus. Between the filter and the pump there is a T-connector with a one way pressure valve adjusted so that if the filter should become clogged the pumped water is merely redirected to the intake side of the pump. A pressure gauge is placed in-line before the filter to indicate whether or not water is being pumped through the filter. The filters used to clean the water are Nuclepore 0.4 μm (N040 CPR 047 00) and 5.0 μm (N 500 CPR 047 00) and Millipore 0.3 μm (PHWP 047 00). First the 5.0 μm filter is used, then the 0.4 μm filter and finally the 0.3 μm filter. After passing through the filters the water passes through tubing to the top of the cell. The water is removed from the cell at the end opposite from where the water comes back in after being filtered. In this way it is reasonable to assume that the whole sample of water in the cylindrical scattering cell gets filtered as quickly as possible.

E. Receiver

The light detection unit is composed of a neutral density filter, a pinhole, a light stop, an opal glass diffuser and a photomultiplier tube. The neutral density filter has a filter factor of 5×10^{-6}. It is used only when the receiver is scanning the main beam (unscattered radiant intensity) and it is used because the intensity of the main beam is approximately six orders of magnitude greater than the intensity received at small angles from the main beam. Therefore, in order to use the same scale on the recorder to measure intensity of the main beam and scattered intensity at small angles it is necessary to put a filter of high neutral density in front of the main beam. The pinhole is needed to minimize the area of reception of scattered light. The larger the area, the larger the plane angle of reception. With a large plane angle of reception the error in the measured angle of scattering is large as shown in Figure 17. The error in angular measurement is given in the Figure by:

$$\frac{\Delta\theta}{\theta + \Delta\theta}$$

Obviously as the diameter, D, of the receiver pinhole increases, $\frac{\Delta\theta}{\theta + \Delta\theta}$ will increase. The same will occur if r decreases. For this reason a small diameter pinhole placed a large distance from the scattering source is used in this experiment. Specifically:

$r = 1000$ mm, $D = 1$ mm, therefore,

$$r \sin(\Delta\theta) = D$$

but

$$\Delta\theta \ll 1 \quad \therefore \sin \Delta\theta \cong \Delta\theta$$

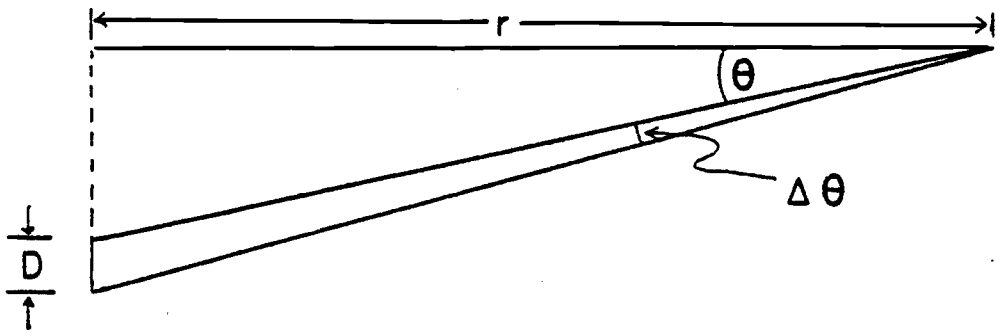

Fig. 17. Effect of receiver area on angular error.

$$r\Delta\theta = D$$

$$\Delta\theta = 0.001 \text{ radians} = 0.057°$$

$$\text{in this experiment } 0.1° \leq \theta \leq 0.55°$$

Therefore the error, $\frac{\Delta\theta}{\theta + \Delta\theta}$ will have a mean value of 0.1485 or approximately 15%. That is, the values of θ used in this experiment are correct to within approximately 15%.

The light stop of 2.5 mm diameter is used for aligning the receiver unit with the main beam. The stop acts as a tube allowing light to be detected only when the receiver is correctly aligned.

The opal glass diffuser serves to diffuse the received light over a larger area of the photomultiplier tube. This is done to prevent any problems in regard to using too small an area of the photomultiplier tube detection surface. Often the coatings on these surfaces are not perfectly uniform so the larger the area utilized the more consistent the results.

The photomultiplier tube is an RCA type PF1023, 10 dynode photomultiplier tube. The photocathode on the tube is an Extended Red Multi-Alkali (ERMA) having a spectral response better than a conventially processed multialkali photocathode. Specifically, the ERMA photocathode has a typical absolute sensitivity of 3.1×10^{-2} $\frac{\text{amps}}{\text{watt}}$ at a wavelength of 632.8 nm, while a conventially processed multialkali photocathode typically has an absolute sensitivity of approximately 2.0×10^{-2} $\frac{\text{amps}}{\text{watt}}$ at the same wavelength. The photomultiplier tube operates on a $\pm$ 12VDC power source.

F. Control Electronics and recorder

The control electronics consists of the circuitry necessary to convey the signal from the PM tube to the Y-axis of the X-Y recorder and also the motor electronics used to drive the platform on which the PM tube is mounted. The same power supply used to drive this platform also drives the X-axis of the X-Y recorder at the same time. The recorder used is a Hewlett-Packard Moseley 7005B X-Y Recorder.

Particle size analysis

A. Particle size analyzer

The experimental work involving the determination of specific particle size distributions is performed here using a combination of particle counter glassware and a pulse height analyzer (Figure 18). The glassware is manufactured by the Coulter Electronics Sales Company and the pulse height analyzer is a model ND2400 manufactured by Nuclear Data, Inc. in conjunction with a Hewlett-Packard 1208 B oscilloscope. An in-depth discussion of the theory behind particle size determinations using Coulter glassware can be found in Sheldon and Parsons (1967). Basically, the sample to be tested, consisting of particles suspended in a conducting medium, is drawn through a very small aperture in a glass tube at a given rate of flow. Every time a particle passes through the aperture a pair of electrodes detects a resistance change across the aperture. The extent of change in resistance depends on the type of material the particle is composed of and on the size of the particle. All of the particles used in this experiment are of the same material (polystyrene divinyl benzene) so only the particles can cause resistance changes. The corresponding resistance "pulse" is sent to the ND2400 pulse height analyzer and the oscilloscope and cumulative counts of particles within given size ranges (or resistance pulse ranges) are made. With the setup used here the size ranges, also called windows, were approximately 0.26 μm each. The aperture in the glassware for this experiment is 100 μm and the flow rate is $3.1 \times 10^{-2} \ \frac{ml}{sec}$.

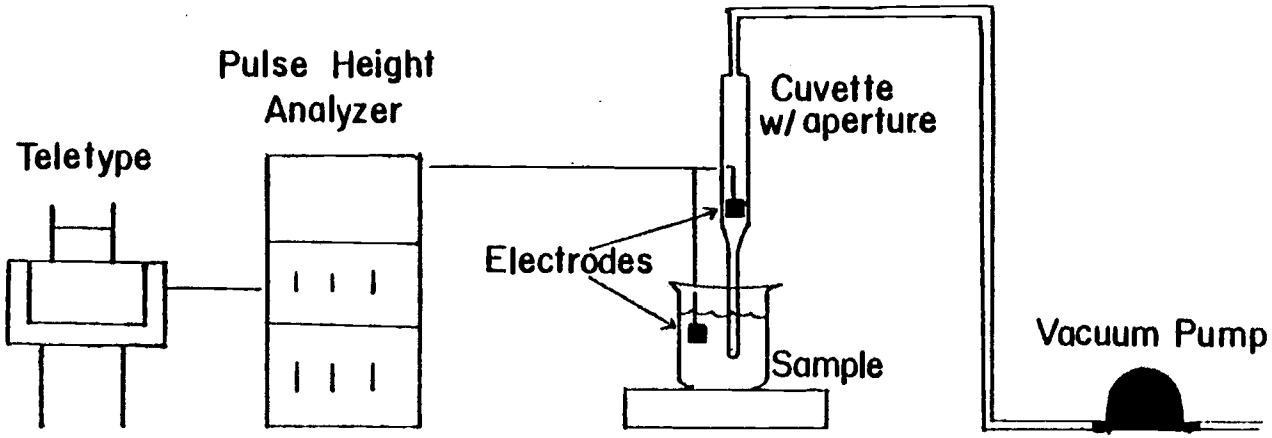

Fig. 18. Schematic drawing of the particle size analyzer.

B. Particles

The particles used in this experiment are spheres of polystyrene divinyl benzene suspended in water. They are supplied by Particle Information Services of Grants Pass, Oregon. The diameters of the particles in use for this experiment are 5.2 μm (standard deviation of 0.36 μm), 8 μm (standard deviation of 1.20 μm), and 9.8 μm (standard deviation of 1.23 μm). They all have an index of refraction of 1.15 relative to pure water. Particles of these three sizes are chosen because particles larger than 1-2 μm are responsible for scattering in water. Also, by using particles of diameter smaller than 20 μm problems with settling of the particles during experimentation can be avoided. In the cases of all three particle sizes used the settling (Stokes') velocity is less than $3 \times 10^{-7} \frac{m}{sec}$ and the running time for the experiment is on the order of 10^3 seconds so settling can be neglected.

IV EXPERIMENTAL PROCEDURE

Particle Size Analysis

The particles used for the experiment are first mixed with 300 ml of distilled, double filtered water (filtered through a 0.8 μm filter and a 0.3 μm filter) to create stock particle concentrations. In each case for the three particle sizes approximately forty drops of the concentrated particle suspensions as packaged by the distributor are added to the filtered, distilled water to make the stock particle concentration. A beaker is then filled with 100 ml of filtered, saline water and it is placed in the particle size analyzer for 100 seconds. Five separate trials are made of this "blank" sample. After running the "blank" sample, its volume is reduced to 90 ml and a volume of the particle concentration equal to 10 ml is added to the clean water. The purpose of this is to create a sample for analysis which has exactly one-tenth the particle concentration per ml of the actual stock particle concentrations. The beaker is then placed in the particle size analyzer and five separate analyses are made. The stock particle concentration cannot be counted directly because it has distilled water as the suspending medium. To use the particle size analyzer the suspending medium must be electrically conducting. This procedure is used for each of the three particle sizes. The actual particle count per size range on the particle size analyzer is obtained by subtracting the particle count per window (or size range) of the "blank" sample from the particle count per corresponding window for the sample containing the 10 fold dilution of the stock particle concentration. The flow rate is 3.1×10^{-2} $\frac{\text{ml}}{\text{sec.}}$ and

each sample is run for 200 sec. so the volume of sample tested is approximately 6.2 ml. If the number of particles per window in the particle size analyzer is divided by 6.2 ml then the approximate particle concentration (in terms of particles per milliliter) for each particle size may be determined. Obviously, since five "blank" samples and five particulate-containing samples are tested then there will be maximum, minimum and mean values of the true particle concentration. The values obtained for the particle concentration are then multiplied by ten to obtain the particle concentration of the stock supplies (recall these had been diluted for use in the particle size analyzer).

Narrow Angle Scattering Measurement

The first necessary step in using the narrow angle scattering meter is to correctly align and clean all the equipment. The optical set-up is aligned by adjusting the pinhole near the laser to obtain a beam of light that is even and free of diffraction patterns. The lenses and scattering cell must be cleaned first with a solution of soap and warm water, then methanol, then distilled water. They are then wiped dry. These components must be kept extremely clean. A single dust particle on the outside surface of a lens can cause experimental measurement errors in $\beta(\theta)$ of up to an order of magnitude. A dust particle on the inside of a lens provides a nucleus of formation for bubbles which can drastically alter results. The scattering cell is then filled with pure distilled, filtered (5 μm filter, 0.8 μm filter and 0.3 μm filter) water and it is aligned so that any reflections off the lenses are directed back along the optical axis of the system. The photomultiplier tube is aligned by placing it directly in the main beam. A mirror is then placed flat across the front edge of the detector and the reflected main beam is aligned to coincide with the incident main beam. During this whole process the laser, scattering cell, and detector unit are each leveled with a bubble level.

The water in the scattering cell is then pumped through the in-line filtration system until it reaches what shall be called the "standard clean water scattering level". This level corresponds to a reading of approximately 20 mv on the Y-axis of the X-Y recorder when the X-axis is approximately 0.55° from the main beam. See Figure 19. In all cases this standard clean-water level is less than

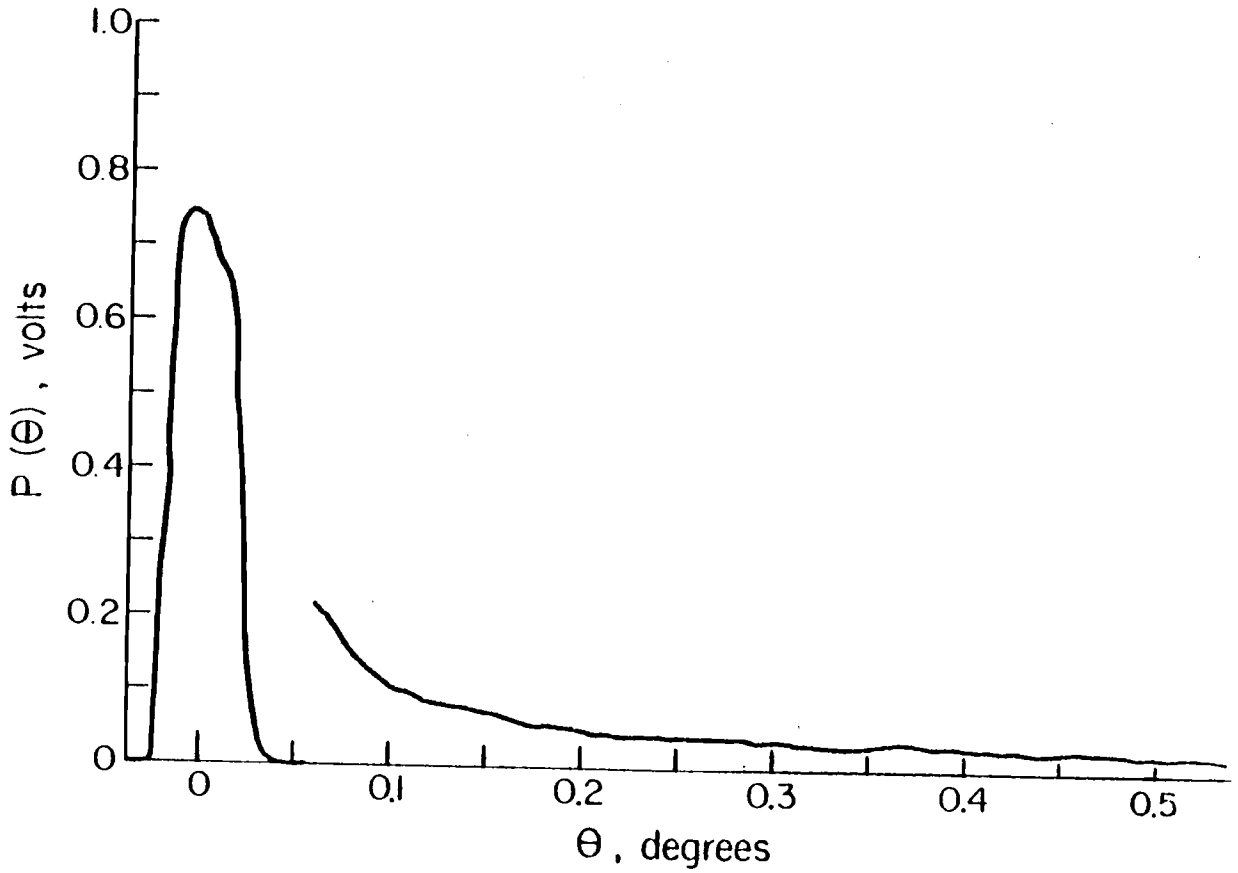

Fig. 19. Standard clean water scattering profile from narrow angle scattering meter.

5% of the scattering level of the samples containing particles.

With the cell nearly full of clean water, 10 ml of the stock particle supply of a given size is injected into the cell with a syringe. The syringe is used to mix the water and the particle stock until a relatively homogeneous suspension is obtained within the cell. The photomultiplier tube then scans the main beam to obtain a value of $P_{r_1}(o)$ for use in equation (27). Figure 20 shows a typical scanning profile. The scanning continues over a distance of approximately 13 mm corresponding to an angular region from 0° to 0.55°. In this way values of $P_{r_1}(\theta)$ are obtained for use in equation (27). The scanning process is repeated four more times to obtain maximum and minimum values of both $P_{r_1}(o)$ and $P_{r_1}(\theta)$. Five experimental trials were found to be a good number of trials. The plots obtained within five trials were quite consistent. Further trials merely duplicated the data received on the first five trials. Five trials were considered to be a large enough number to provide good statistical analysis of the data. Then 10 ml more of the particle stock is added to the cell to make the total amount of particle stock contained in the cell equal to 20 ml, and F (in equation 27) is very nearly equal to two. The whole scanning process is then repeated five more times to obtain maximum and minimum values of $P_{r_2}(o)$ and $P_{r_2}(\theta)$. The water in the cell is then pumped and filtered until the standard clean water scattering level is again attained and the experiment is then performed for another particle size.

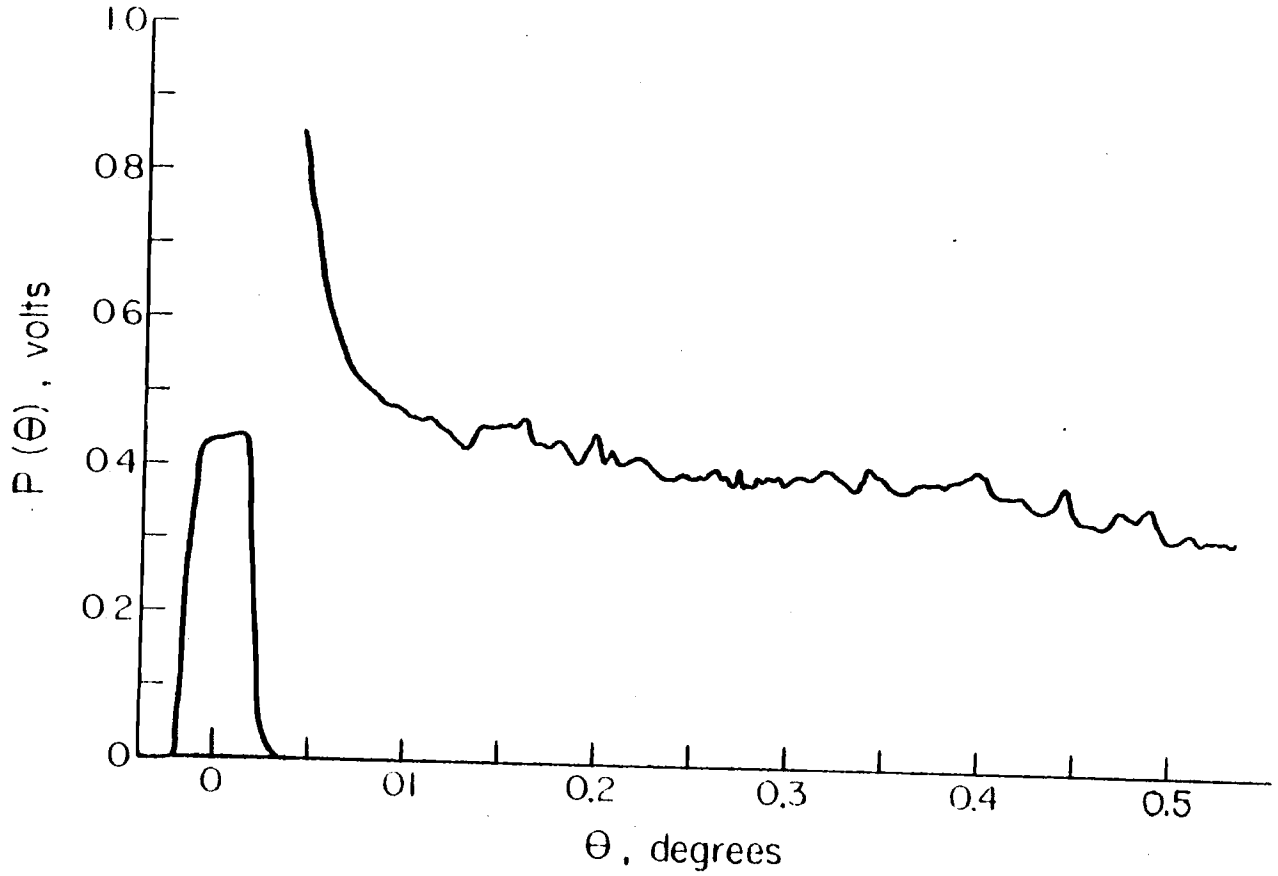

Fig. 20 Typical particulate scattering profile from narrow angle scattering meter.

V RESULTS AND OBSERVATIONS

Theoretical Results From Particle Size Analysis

The FOCAL computer programs used for the theoretical calculations of the volume scattering function are found in Appendix 2. Table 1 shows the particle size distribution for the stock concentration of 5.2 μm diameter particles. Shown are the particle size range and the mean and standard deviation of the number of particles measured per milliliter of stock solution within that size range. The maximum and minimum number of particles per milliliter per size range for five measurements are also shown. Tables 2 and 3 show the same data for the particles with diameters of 8 μm and 9.8 μm respectively. This data provides the value of N for use in equation (4). The values of $i(\theta)$ are obtained from Salganik and Shifrin (1973) and are in terms of one particle per cubic meter. These are then multiplied by 10^6 to obtain 10^6 particles per cubic meter, or one particle per ml. The theoretical volume scattering function for one particle per milliliter is then multiplied by the mean and standard deviation of the number of particles per milliliter in the stock concentration to obtain means and standard deviations of the theoretical volume scattering function. Similarly, the maximum and minimum theoretical volume scattering functions are obtained from the maximum and minimum particle counts per size range. Graphs of the mean and standard deviation of the theoretical volume scattering function versus the angle are shown in Figures 21, 22 and 23 for particle sizes of 5.2 μm, 8 μm and 9.8 μm respectively.

Table 1

STOCK PARTICLE SIZE ANALYSIS OF 5.2 μm DIAMETER PARTICLES

Mean Diameter (μm)	Particles per Milliliter			
	Mean	Standard Deviation	Maximum	Minimum
4.0	1012	560	3123	0
4.4	4426	342	5040	3360
4.8	12342	291	17760	11520
5.2	9092	174	9360	8640
5.6	8300	177	8880	8160
6.0	3821	92	3840	3600
6.5	7129	115	7440	6960
6.9	6113	156	6480	5760
7.3	2716	160	2880	2640
7.7	4423	171	4800	4080
8.1	1789	181	2160	1680
8.5	2715	172	3120	2640
8.9	999	100	1200	960
9.3	791	100	960	720
9.7	597	74	720	480
10.1	465	66	584	389
10.5	320	55	480	240
10.9	237	56	321	168
11.3	184	34	247	134
11.7	114	30	168	74
12.1	90	8	103	76
12.5	68	11	87	47
12.9	46	16	77	26
13.5	30	8	44	13
14.1	19	7	34	13
14.5	11	11	34	3
14.9	9	6	16	0
15.3	0	0	0	0
15.7	5	3	15	0
16.1	5	4	15	0
16.5	0	0	0	0
16.9	3	3	8	0
17.3	4	3	10	0
17.7	0	0	0	0
18.1	3	3	10	0
18.5	0	0	0	0
18.9	2	2	7	0
19.3	1	1	5	0
19.7	0	0	0	0
20.1	0	0	0	0
21.2	0	0	0	0
22.2	0	0	0	0
23.2	0	0	0	0

Table 2

STOCK PARTICLE SIZE ANALYSIS OF 8 μm DIAMETER PARTICLES

Mean Diameter (μm)	Particles per Milliliter			
	Mean	Standard Deviation	Maximum	Minimum
3.6	166	20	205	127
4.0	510	48	653	383
4.4	271	43	379	177
4.8	443	44	544	290
5.2	617	29	700	561
5.1	1602	64	1755	1495
6.0	1690	42	1752	1623
6.5	7940	166	8363	7718
6.9	17404	323	17874	16747
7.3	12105	189	12381	11800
7.7	25559	313	26158	24989
8.1	11266	324	11897	10950
8.5	16802	344	17605	16294
8.9	5245	238	5639	5005
9.3	3425	158	3698	3253
9.7	2083	123	2329	1995
10.1	1166	104	1368	1052
10.5	602	59	708	540
10.9	285	31	337	234
11.3	126	7	137	113
11.7	52	7	63	40
12.1	22	4	29	13
12.5	10	7	21	0
12.9	7	4	13	0
13.3	2	2	6	0
13.7	0	0	0	0
14.1	1	1	6	0
14.5	1	1	3	0
14.9	0	0	0	0
15.3	1	1	5	0
15.7	1	1	5	0
16.1	0	0	0	0
16.5	1	1	3	0
16.9	1	1	5	0
17.3	0	0	0	0
17.7	2	1	3	0
18.1	0	0	0	0
18.5	2	2	6	0
18.9	1	1	3	0
19.3	0	0	0	0
19.7	1	1	3	0
20.1	1	1	3	0
21.2	0	0	0	0
22.2	2	1	3	0
23.2	0	0	0	0

Table 3

STOCK PARTICLE SIZE ANALYSIS OF 9.8 μm DIAMETER PARTICLES

Mean Diameter (μm)	Particles per Milliliter			
	Mean	Standard Deviation	Maximum	Minimum
3.6	22	39	132	0
4.0	142	52	295	0
4.4	36	19	100	0
4.8	32	19	100	0
5.2	26	20	94	0
5.6	15	11	32	0
6.0	31	6	40	19
6.5	308	22	358	277
6.9	1560	63	1711	1413
7.3	1741	111	1861	1550
7.7	6196	234	6681	5689
8.1	4744	232	5118	4374
8.5	14263	531	15165	12969
8.9	10021	474	10598	9287
9.3	11033	571	11748	10079
9.7	10337	467	10861	9523
10.1	7646	223	7955	7563
10.5	4191	105	4358	4023
10.9	1724	27	1756	1681
11.3	603	17	626	573
11.7	225	20	258	197
12.1	104	9	116	84
12.5	54	9	69	40
12.9	28	5	37	21
13.3	18	8	34	11
13.7	0	0	0	0
14.1	14	4	19	6
14.5	7	4	13	5
14.9	0	0	0	0
15.3	6	5	16	2
15.7	3	2	6	0
16.1	0	0	0	0
16.5	5	2	6	2
16.9	3	2	66	0
17.3	0	0	0	0
17.7	1	1	3	0
18.1	0	0	0	0
18.5	1	1	3	0
18.9	1	1	2	0
19.3	0	0	0	0
19.7	1	0	2	0
20.1	1	1	5	0
21.2	0	0	0	0
22.2	0	0	0	0
23.2	0	0	0	0

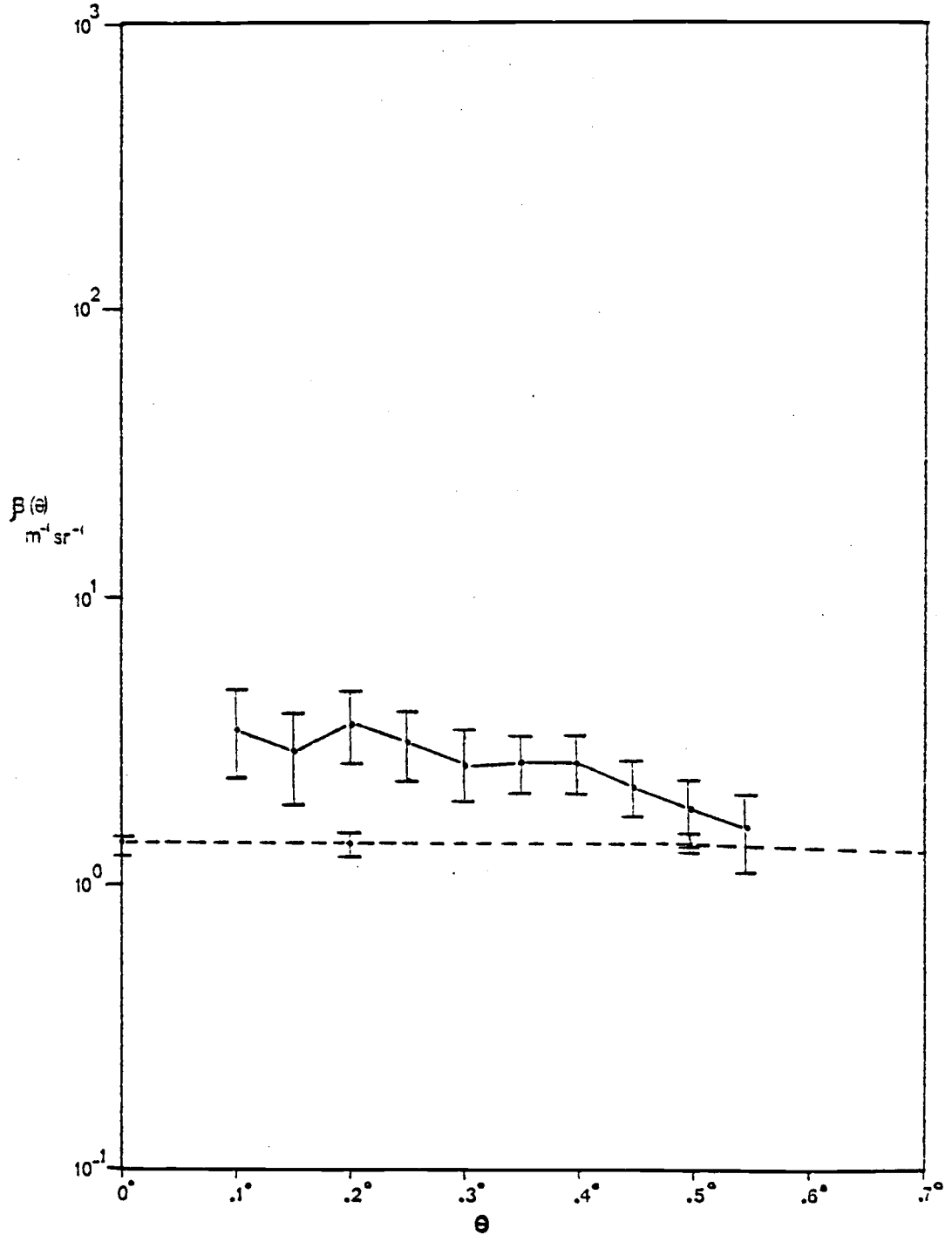

Fig. 21 Experimental (solid line) and theoretical (dashed line) volume scattering functions of the 5.2 μm diameter particles. Shown are the mean values plus and minus one standard deviation.

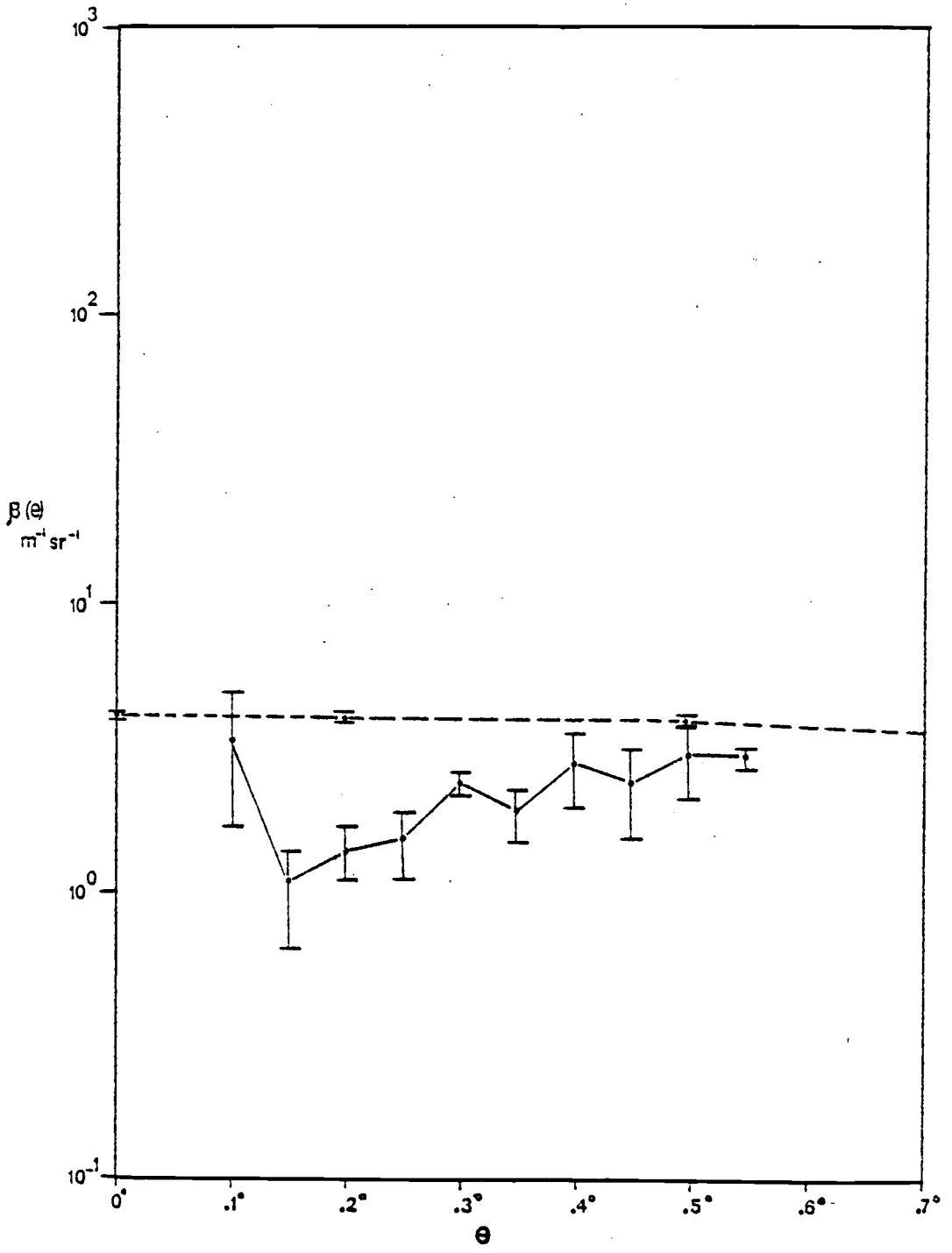

Fig. 22 Experimental (solid line) and theoretical (dashed line) volume scattering functions of the 8 μm diameter particles. Shown are the mean values plus and minus one standard deviation.

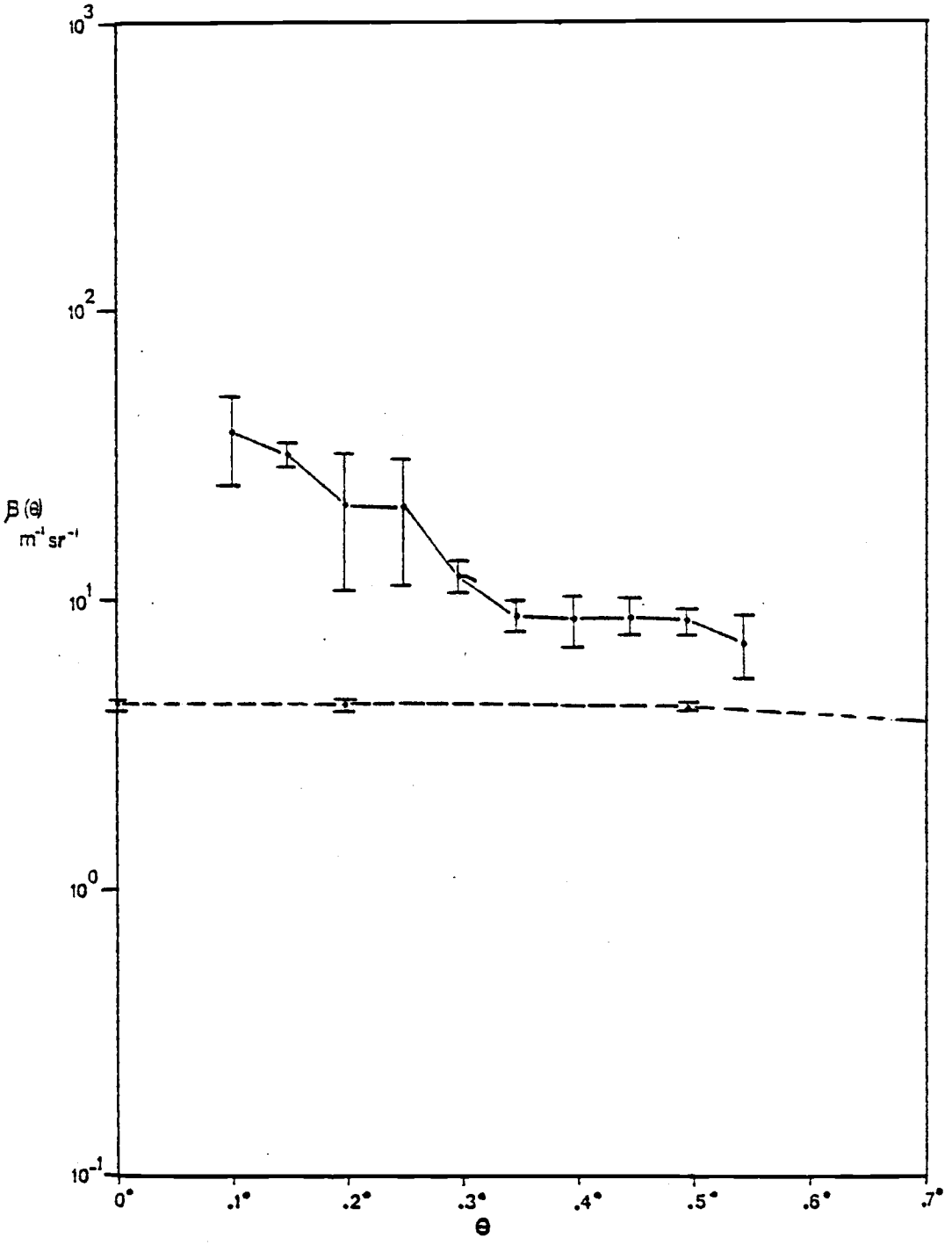

Fig. 23 Experimental (solid line) and theoretical (dashed line) volume scattering functions of the 9.8 μm diameter particles. Shown are the mean values plus and minus one standard deviation.

The graphs of the maximum and minimum values of the theoretical volume scattering function are shown in Figures 24, 25 and 26 for the same respective particle sizes. In addition, the values of the theoretical volume scattering functions are shown in Tables 4, 5 and 6 for the 5.2 μm, 8 μm and 9.8 μm particles respectively.

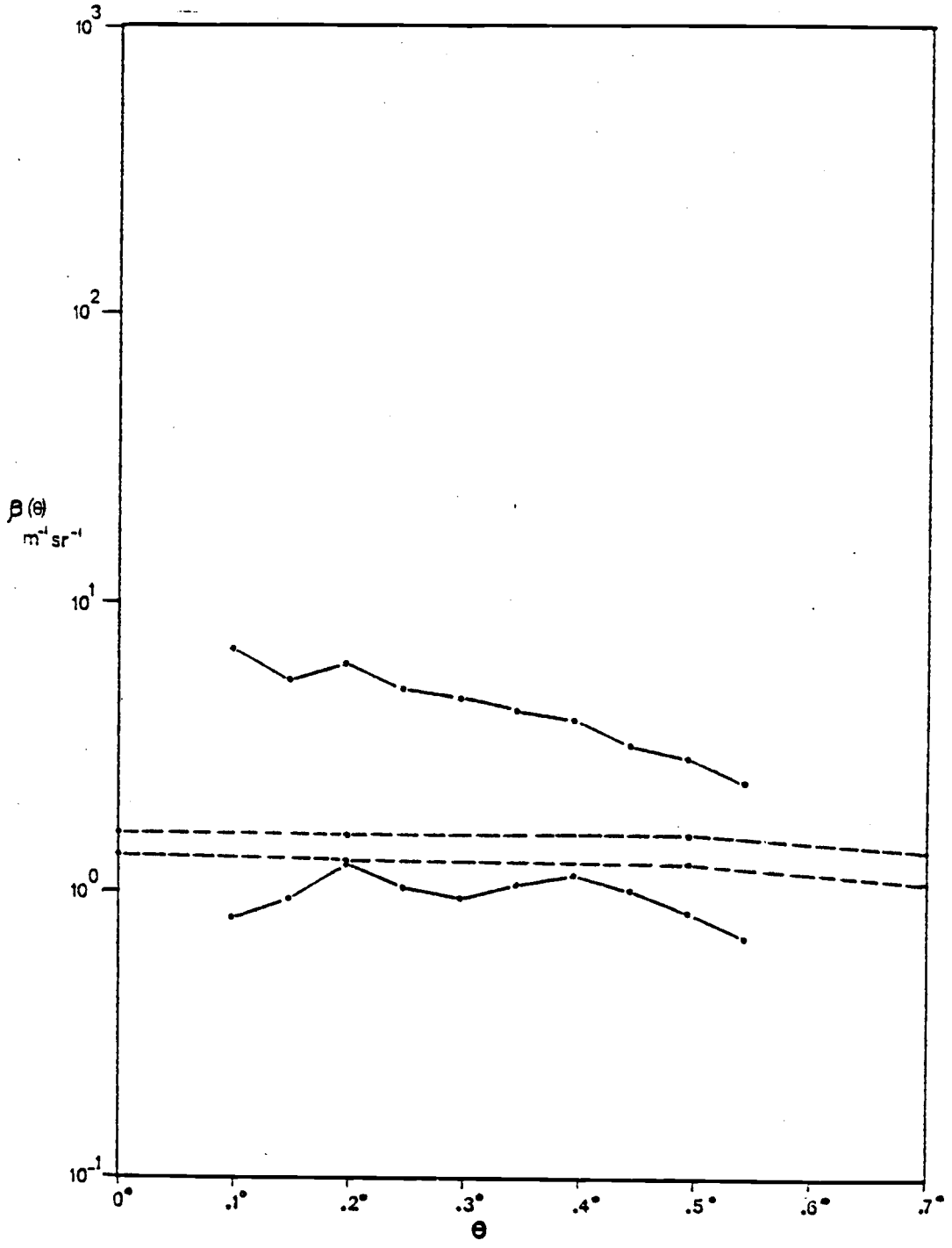

Fig. 24 Experimental (solid line) and theoretical (dashed line) volume scattering functions of the 5.2 μm diameter particles. Shown are the maximum and minimum theoretical and experimental values.

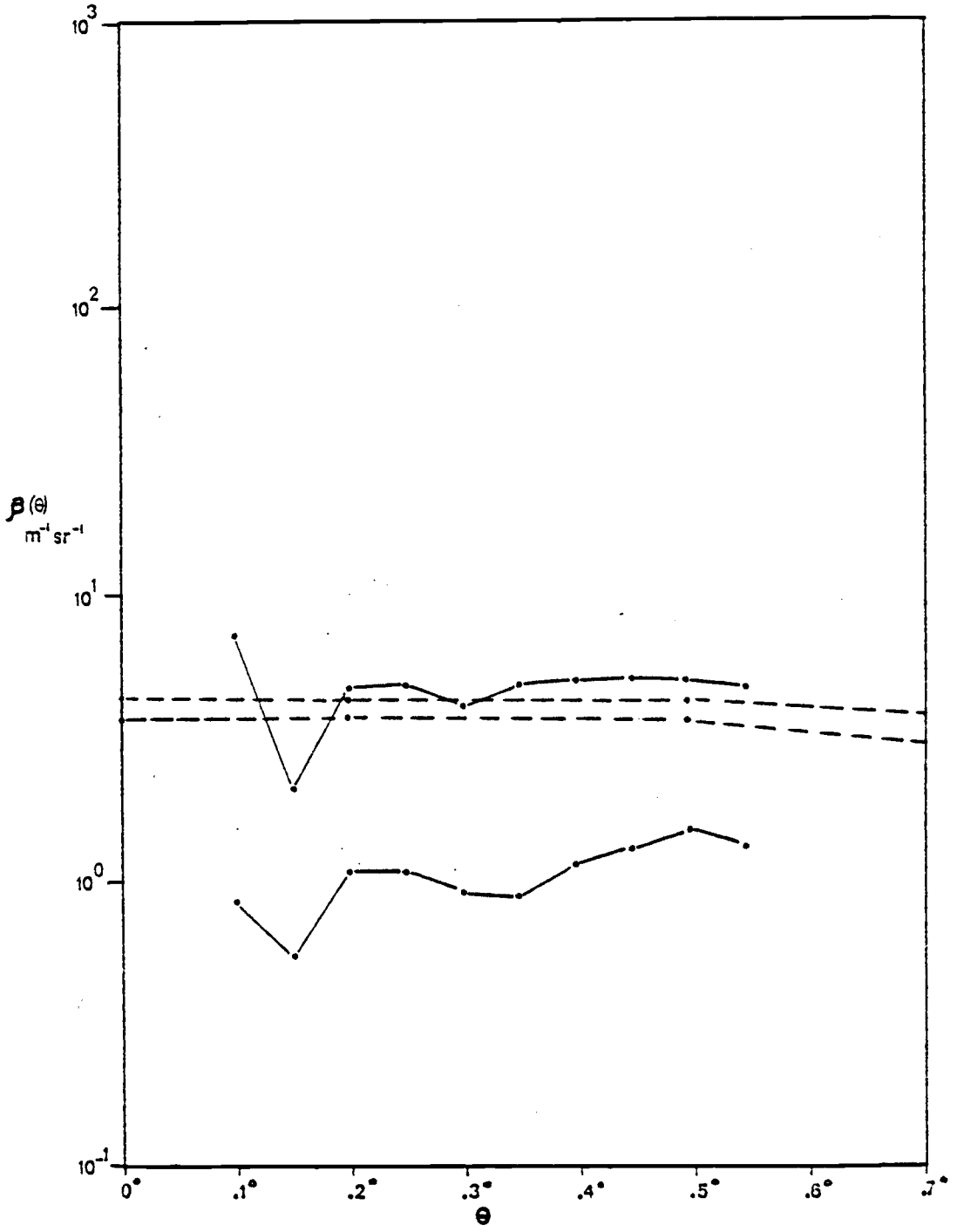

Fig. 25 Experimental (solid line) and theoretical (dashed line) volume scattering functions of the 8 μm diameter particles. Shown are the maximum and minimum theoretical and experimental values.

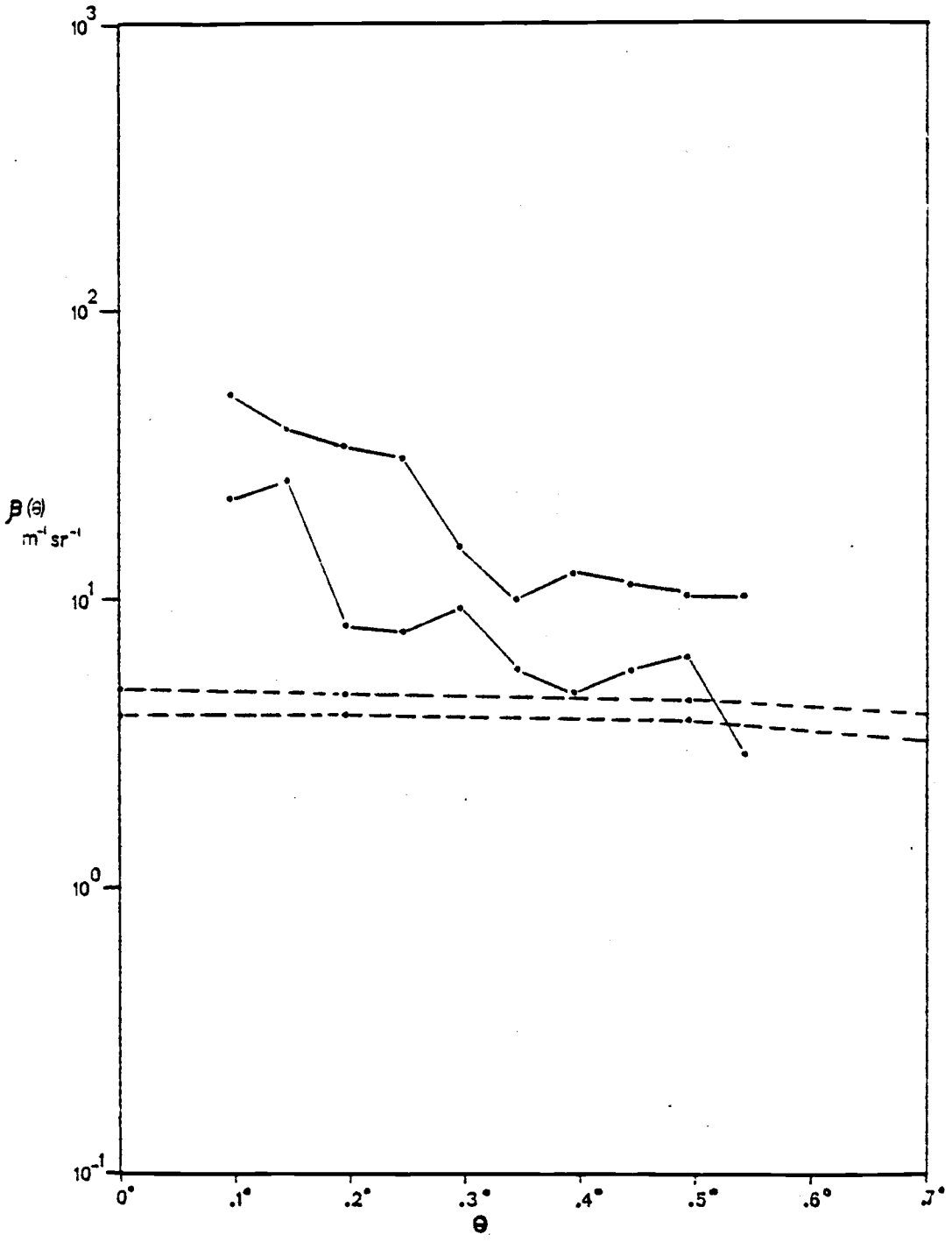

Fig. 26 Experimental (solid line) and theoretical (dashed line) volume scattering functions of the 9.8 μm diameter particles. Shown are the maximum and minimum theoretical and experimental values.

Table 4

THEORETICAL VOLUME SCATTERING FUNCTION FOR 5.2 μm PARTICLES

Angle, θ	Mean	Standard Deviation	Maximum	Minimum
0°	1.40	0.11	1.48	1.26
0.2°	1.40	0.12	1.51	1.24
0.5°	1.36	0.11	1.47	1.21
1°	1.00	0.08	1.08	0.89

Table 5

THEORETICAL VOLUME SCATTERING FUNCTION FOR 8 μm PARTICLES

Angle, θ	Mean	Standard Deviation	Maximum	Minimum
0°	4.08	0.12	4.27	3.88
0.2°	4.07	0.12	4.25	3.86
0.5°	3.94	0.12	4.12	3.75
1°	3.18	0.09	3.32	3.03

Table 6

THEORETICAL VOLUME SCATTERING FUNCTION FOR 9.8 μm PARTICLES

Angle, θ	Mean	Standard Deviation	Maximum	Minimum
0°	4.32	0.18	4.73	4.16
0.2°	4.32	0.18	4.53	3.96
0.5°	4.14	0.18	4.34	3.80
1°	3.03	0.13	3.19	2.77

Experimental Results From the Narrow Angle Scattering Meter

The FOCAL program used to calculate the experimental volume scattering functions is found in Appendix 2. By using five trials on the narrow angle scattering meter for each concentration of particles there is obviously a large range of possible values of $\frac{P_{r_2}(\theta)}{P_{r_2}(o)} - \frac{P_{r_1}(\theta)}{P_{r_1}(o)}$. With five plots obtained for each particle concentration there are twenty-five possible values of $\frac{P_{r_2}(\theta)}{P_{r_2}(o)} - \frac{P_{r_1}(\theta)}{P_{r_1}(o)}$.

Table 7 shows the maximum, minimum, mean value and standard deviation of this subtraction as a function of θ for the experiment with the 5.2 μm particles. Tables 8 and 9 show the same for the 8 μm and 9.8 μm particles respectively. These values are used in equation (27) to obtain the maximum, minimum, mean and standard deviation of the experimental volume scattering function. In addition, for use in equation (27), the solid angle, ω_θ, equals 7.85×10^{-7} sr; L = 0.5 m: F = 2. Figure 21 shows the experimentally obtained mean values of $\beta(\theta)$ plus and minus one standard deviation for θ from 0.1° to 0.55° and for the 5.2 μm particle. Figures 22 and 23 show the same results for the 8 μm particles and 9.8 μm particles. Figures 24, 25 and 26 show the experimentally obtained maximum and minimum values of $\beta(\theta)$ vs. θ for the 5.2 μm, 8 μm and 9.8 μm particles respectively.

Table 7

EXPERIMENTALLY OBTAINED VALUES OF $\frac{P_2(\theta)}{P_2(o)} - \frac{P_1(\theta)}{P_1(o)}$ FOR 5.2 μm PARTICLES

	$(x10^{-6})$			
Angle, θ	Mean	Standard Deviation	Maximum	Minimum
0.1°	1.41	0.29	2.61	0.30
0.15°	1.16	0.31	2.05	0.35
0.2°	1.47	0.25	2.33	0.49
0.25°	1.24	0.26	1.86	0.38
0.3°	1.04	0.15	1.78	0.36
0.35°	1.06	0.22	1.61	0.40
0.4°	1.06	0.20	1.50	0.43
0.45°	1.06	0.20	1.50	0.43
0.5°	0.72	0.17	1.11	0.31
0.55°	0.61	0.17	0.92	0.25

Table 8

EXPERIMENTALLY OBTAINED VALUES OF $\frac{P_2(\theta)}{P_2(o)} - \frac{P_1(\theta)}{P_1(o)}$ FOR 8 μm PARTICLES

	$(x10^{-6})$			
Angle, θ	Mean	Standard Deviation	Maximum	Minimum
0.1°	1.32	0.70	2.89	0.33
0.15°	0.40	0.15	0.84	0.21
0.2°	0.54	0.12	1.86	0.43
0.25°	0.60	0.16	1.92	0.43
0.3°	0.95	0.09	1.62	0.37
0.35°	0.75	0.16	1.95	0.35
0.4°	1.10	0.32	2.00	0.45
0.45°	0.93	0.32	2.00	0.51
0.5°	1.18	0.35	1.97	0.59
0.55°	1.15	0.09	1.87	0.52

Table 9

EXPERIMENTALLY OBTAINED VALUES OF $\frac{P_2(\theta)}{P_2(o)} - \frac{P_1(\theta)}{P_1(o)}$ FOR 9.8 μm PARTICLES

	$(x10^{-6})$			
Angle, θ	Mean	Standard Deviation	Maximum	Minimum
0.1°	14.96	5.22	20.73	12.88
0.15°	12.57	1.04	15.65	10.49
0.2°	8.37	4.17	13.45	3.15
0.25°	8.25	3.79	12.00	3.11
0.3°	4.65	0.49	6.05	3.73
0.35°	3.41	0.44	3.85	2.24
0.4°	3.33	0.33	4.77	1.87
0.45°	3.38	0.47	4.37	2.24
0.5°	3.24	0.23	3.98	2.46
0.55°	2.72	0.53	4.08	1.11

VI DISCUSSION AND CONCLUSION

In Figures 21 through 26 the theoretical and experimental results of this experiment are compared. Figures 21, 22 and 23 show the comparison of mean and standard deviation values of experimental and theoretical $\beta(\theta)$ vs. θ for 5.2 μm, 8 μm, and 9.8 μm particles respectively. Figures 24, 25 and 26 compare the experimental and theoretical maximum and minimum values of $\beta(\theta)$ vs. θ for 5.2 μm, 8 μm, and 9.8 μm particles respectively.

From these curves it is apparent that the narrow angle scattering meter can effectively measure the scattered radiant intensity at angles less than 0.55°. The results obtained indicate that the behavior of scattered light as predicted by Mie (1908) is, in fact, a verifiable phenomenon. The flatness of the curve of $\beta(\theta)$ vs. θ is seen experimentally and theoretically. The normalized results of this experiment (normalized to $\beta(\theta) = 1\ m^{-1}sr^{-1}$ at $\theta = 0.1°$, 0.3° and 0.5°) have been calculated and the mean normal results of the three particle sizes are shown compared to the normalized results of other experimentalists in Figures 27, 28 and 29. The experimentally obtained slopes of $\beta(\theta)$ vs. θ agree very well with those that theory predicts. Any slight deviations in slope from what theory predicts may be explained by the appearance of large particles such as dust or microbubbles in the scattering meter sample cell. Figure 11 shows what the theoretical scattering would be for a particle size distribution containing both large and small particles. Since the scattered radiant intensity decreases more rapidly at smaller angles for large particles, a sample containing both large and small particles will exhibit a significant

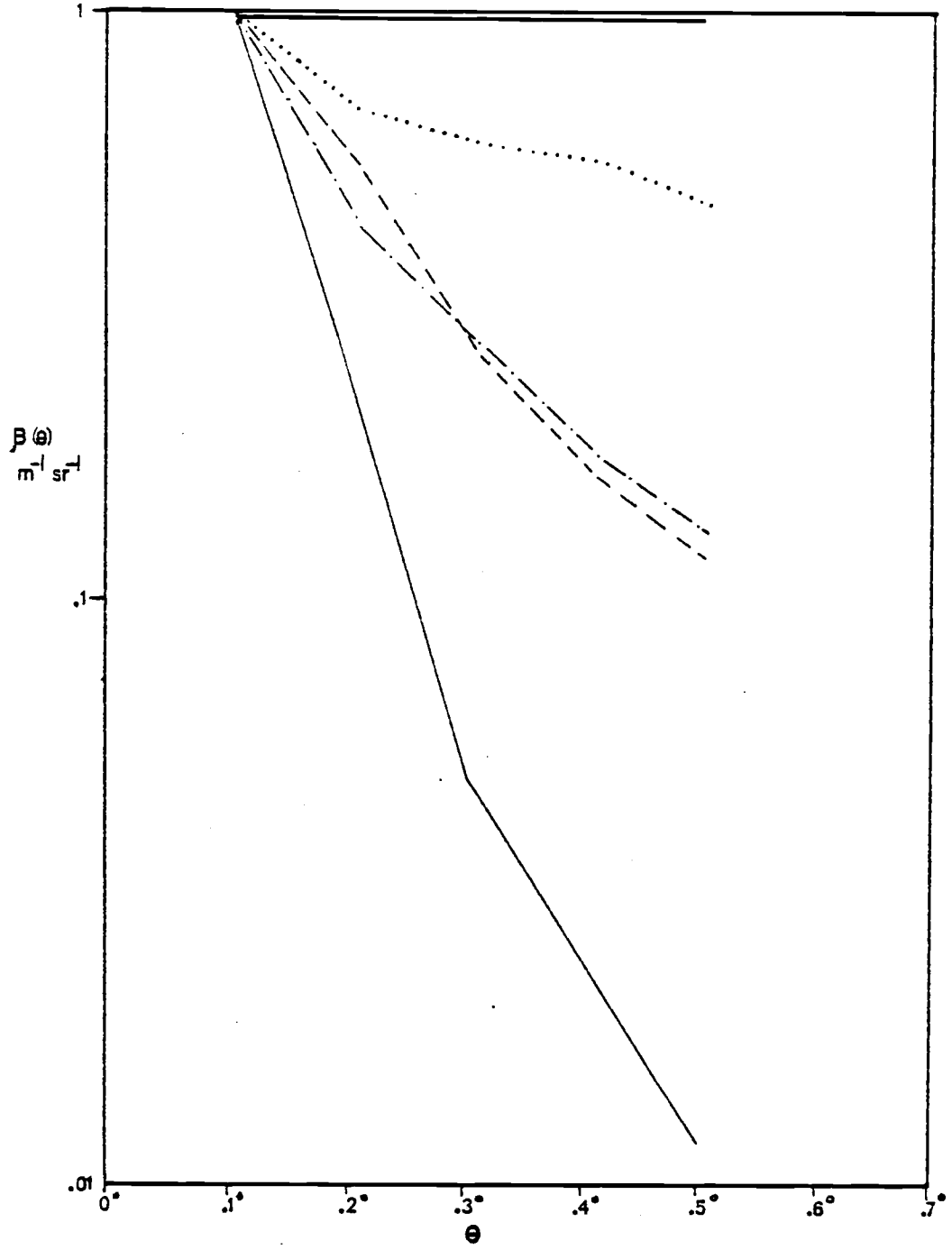

Fig. 27 Comparison of results from this experiment (dotted line) to results of Hodara (1973; thin solid line), Petzold (1972; dashed line), Morrison (1967; dots and dashed), and Mie (1908) theory (thick solid line). Results are normalized to $\beta(\theta) = 1 m^{-1} sr^{-1}$ at 0.1°.

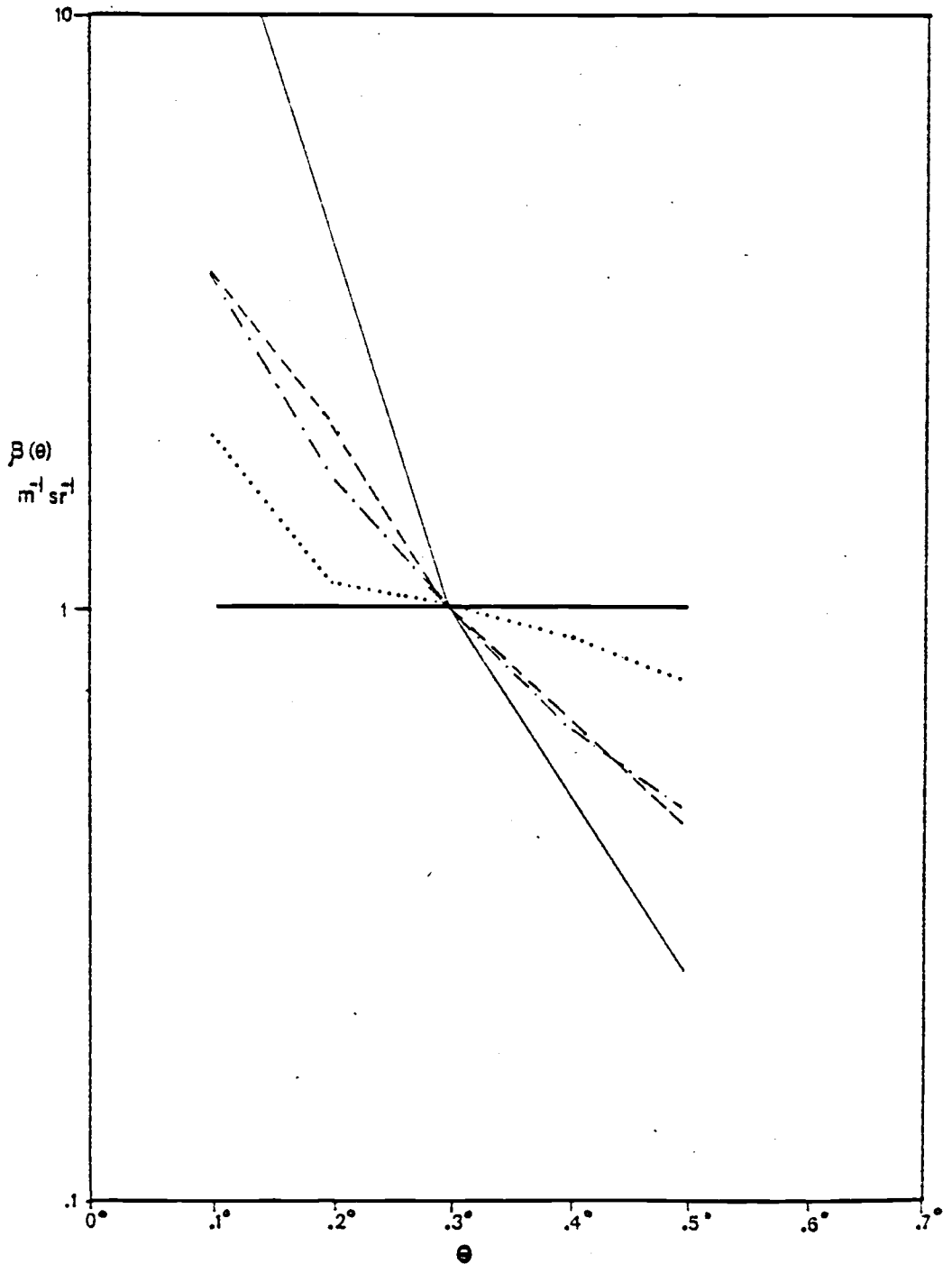

Fig. 28 Comparison of results from this experiment (dotted line) to results of Hodara (1973; thin solid line), Petzold (1972; dashed line), Morrison (1967; dots and dashed), and Mie (1908) theory (thick solid line). Results are normalized to $\beta(\theta) = 1 m^{-1} sr^{-1}$ at 0.3°.

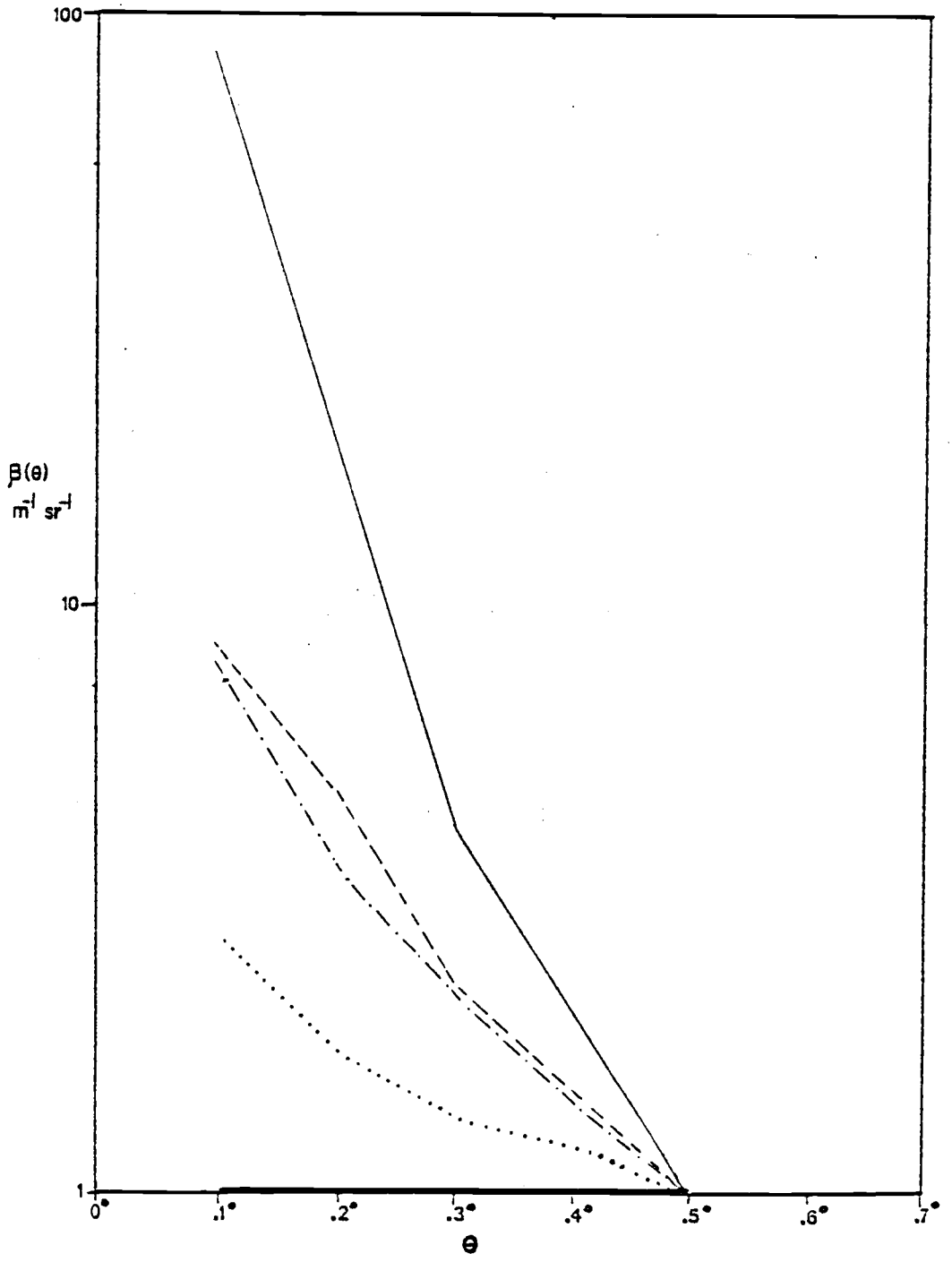

Fig. 29 Comparison of results from this experiment (dotted line) to results of Hodara (1973; thin solid line), Petzold (1972; dashed line), Morrison (1967; dots and dashed), and Mie (1908) theory (thick solid line). Results are normalized to $\beta(\theta) = 1 m^{-1} sr^{-1}$ at 0.5°

slope in $\beta(\theta)$ vs. θ. The 9.8 μm particle scattering curve demonstrates this. In the volume scattering function curves of the 5.2 μm particles and the 8 μm particles both the slopes and the actual values of $\beta(\theta)$ demonstrate excellent agreement of experiment and theory. Slight discrepancies and anomalies in the curves may be explained by a variety of causes. An inhomogeneous particle concentration in either the particle size analysis sample or in the narrow angle scattering meter cell would cause significant changes in the determination of the theoretical or experimental volume scattering function, respectively. Contamination of the sample in the narrow angle scattering meter cell would result in scattered radiant intensity that could not be accounted for in the theoretical calculation. This contamination could be in the form of dust on the lens or in the sample, or microbubbles in the sample. Human error in the exact measurement of particle stock added to the narrow angle scattering meter cell is another source of error in the experimental calculations. Microbubbles of 40 μm diameter could increase the experimental scattering values by approximately 5% to 10% when their concentration is only $\frac{1}{200}$ of the particulate concentration. Dust particles on the lens are usually quite large in relation to the sample particles. Consequently, a single dust particle may be as large as 0.5 mm (500 μm) and its effect on the scattering could be a 30% to 40% increase. Fortunately, dust particles of this size are usually easily detectable, but smaller particles may also exist and they too would have similar, though smaller effects on the scattering.

Perhaps the most significant contribution to excessive experimental scattering is multiple scattering. For the experimental setup used here,

multiple scattering is assumed to occur when the optical length is greater than 0.3 (Van de Hulst, 1957). The optical length is defined as:

$$\tau = cL$$

where c = the attenuation coefficient as defined in Chapter II.

L = length of scattering meter sample cell

Since L = 0.5 m this implies that multiple scattering will occur at values of c greater than 0.6 m^{-1} for this setup. For the 20 ml sample of particles used in the cell in this experiment the values of c are approximately 1 m^{-1}; multiple scattering therefore must occur.

Woodward (1964) has shown that multiple scattering will begin when the ratio of total particulate volume to suspension volume exceeds 4×10^{-6}. Typically in this experiment the value of this ratio is from 0.7×10^{-6} to 5×10^{-6}. According to Woodward (1964) a volume concentration of 5×10^{-6} would result in as much as a 50% increase above the single-scattering value for the scattered intensity at 0.1°. In addition it must be recalled that, as shown in Figure 10, there is a large range of acceptable values of the theoretical volume scattering function. Between two theoretical calculations from Mie theory, the variation in $\beta(\theta)$ at 0.4°, for example, may be as high as 80%. One can be relatively certain that the ranges of theoretical volume scattering functions and experimental volume scattering functions obtained herein do demonstrate significant overlap.

One can conclude that the narrow angle scattering meter can measure the volume scattering function at near-forward angles for monodisperse systems of particles. In conclusion it would seem that

the meter can be used effectively in vitro for polydisperse systems actually found in the ocean. In this way the volume scattering profile at narrow angles and at larger angles could be obtained (by using also a Brice-Phoenix scattering photometer) to produce a scattering profile ($\beta(\theta)$ vs. θ for $0°<\theta<180°$) for a sample of water containing suspended particulate matter. This scattering profile will vary depending on the particle size distribution, the particles' slopes, and the index of refraction of the particle. Therefore, by use of scattering meters at near forward angles, mid-range angles, and angles greater than 90°, together with a particle size analyzer such as a Coulter Counter, it may be possible to determine the relative composite index of refraction of a given sample of suspended particles (Gordon and Brown, 1971; Zaneveld and Pak, 1973; Zaneveld, et al., 1974).

One can also make the important conclusion that hydrosols having low indices of refraction do scatter electromagnetic radiation at small angles as theory predicts. Until now, the seventy-year-old theory of Mie (1908) has been proven correct and accepted only for large angles. This experiment conclusively shows that Mie theory is correct for the near forward angular region for a variety of sizes of particles when suspended in water.

BIBLIOGRAPHY

Ashley, L.E., and Cobb, C.M., 1958, Single particle scattering functions for latex spheres in water , J. Opt. Soc. Am. 48 : 261

Bauer, D., and Ivanoff, A., 1965, Au sujet de la mésure du coefficient de diffusion de la lumière par les eaux de mer pour des angles compris entre 14° et 1° 30'., Comp. Rend. Ac. Sc., 260: 631

Bauer, D., and Morel, A., 1967, Étude auxs petits angles de l' indicatrice de diffusion de la lumière par les eaux de mer., Ann. Geophys., 23 : 109-123

Brown, O. B., and Gordon, H. R., 1971, Tables of Mie scattering functions for low index particles suspended in water. Univ. of Miami Pub. no. MIAPH-OP-71.5

Chu, C. M. and Churchill, S. W., 1957, Angular distribution coefficients for radiation scattered by a spherical particle , J. Opt. Soc. Am., 47 : 81

Duntley, S. Q., 1963, Light in the Sea, J. Opt. Soc. Am., 53 : 214-233

Gordon, H. R., and Brown, O. B., 1971, Small angle Mie scattering for low index hydrosols, J. Opt. Soc. Am., 61 : 1549

Hodara, H., 1973, Experimental results of small angle scattering , AGARD Lecture Series no. 61 on Optics of the Sea, Neuilly Sur Seine, France

Honey, R. C., and Sorenson, G. P., 1970. Optical absorption and turbulence-induced narrow angle forward scatter in the sea., Electromagnetics of the sea., AGARD Conf. Proc. no. 77: 39.1-39.7

Jerlov, N. G., 1976, Marine Optics, Elsevier Pub. Co., N.Y. 231 pp.

Junge, C. E., 1963, Air Chemistry and Radioactivity, Academic Press, N.Y., 382 pp.

Kozlyaninov, M. V., 1957, New instrument for measuring the optical properties of sea water , Tr. Inst. Okeanol., Akad. Nauk. S.S.S.R., 25 : 134

Kullenberg, G., 1968, Scattering of light by Sargasso Sea water , Deep Sea Research, 15 : 423-432

McCluney, W. R., 1974, Multichannel forward scattering meter for oceanography., Applied Optics, 13 : 548-555

Mertens, L. and Wells, W., 1973, As described by Hodara, H., 1973, Experimental results of small angle scattering., Lecture Series no. 61 on Optics of the Sea, Neuilly Sur Seine, France

Mie, G., 1908, Beiträge zur Optik trüber Medien speziell kolloidalen Metallosungen, Ann. Physik., 25 : 377-389

Morel, A., 1966, Étude experimentale de la diffusion de la lumière par l' eau les solutions de chlorure de sodium et l' eau de mer optiquement pures., J. Chim. Phys., 10 : 1359-1366

Morel, A., 1973a, Diffusion de la lumière par les eaux de mer: Resultats expérimentaux et approche théoretique., AGARD Lecture Series no. 61 on Optics of the Sea, 3.1-1 to 3.1-76

Morel, A., 1973b, Indicatrices de diffusion calculées par la théorie de Mie pour les systemes polydisperses, en vue de l' application aux particules marines., Rapport no. 10, Laboratoire d'Océanographie Physique (Université de Paris VI-CNRS), 75 p.

Morrison, R. E., 1967, Studies on the optical properties of seawater, Argus Island in the North Atlantic Ocean and in Long Island and Block Island Sounds, Ph.D. Thesis, New York University, N.Y., 108 pp.

Nyfeller, F., 1970, Etude de la diffusion de la lumiere par l' eau de mer. Mesures aux petits angles a l' aide de sources classiques et de sources lasers., Electromagnetics of the Sea. AGARD Conf. Proc. no. 77 : 31.1.8

Ochakovsky, Y. E., 1966, On the comparison of measured and calculated scattering indicatrices of sea water., U.S. Dept. Comm. Joint Publ. Res. Ser. Rep., 36(816) : 98-105

Pangonis, W. J. and Heller, W., 1960, Angular scattering functions for spherical particles, Detroit, Wayne State Univ. Press, 222 pp.

Petzold, T. J., 1972, Volume scattering functions for selected ocean waters, Scripps Inst. Oc. Ref. 72-78 : 79 pp.

Roach, D. M., 1974, The determination of refractive index distributions for oceanic particulates, Ph.D. Thesis, Oregon State University, Corvallis, Oregon, 173 pp.

Salganik, I. N. and Shifrin, K. S., 1973, Light Scattering Tables, Vol. 5., U.S.S.R. Acad. of Sci, P. P. Shirshkov Inst. of Oceanog, Leningrade, 220 pp.

Sheldon, R. W. and Parsons, T. R., 1967, A practical manual on the use of the Coulter Counter in marine science. Coulter Electronics Sales Co., Canada, 66 pp.

Softley, E. J. and Dilley, J. F., 1972, In situ measurements of small and large angle volume scattering of light in the sea. Ocean 73 : IEEE Int'l Conf. of Engineering in the ocean environment, New Port

Sokolov, R. N., Kudryavitskiy, F. A. and Petrov, G. D., 1971, Submarine laser instrument for measuring the size spectra of particles suspended in sea water., Izv. Atmos. Oceanic Pfys., 7 : 1015-1018

Van De Hulst, H. C., 1957, Light scattering by small particles., Wiley, N.Y., 470 pp.

Wells, W., Hodara, H. and Wilson, O., 1972, Long range vision in sea water., Final Report ARPA order 1737, Tetra Tech Inc. Pasadena, Cal., 155 pp.

Woodward, D. H., 1964, Multiple light scattering by spherical dielectric particles., J. Opt. Soc. Am., 54 : 1325

Zaneveld, J. R. V. and Pak, H., 1973, Method for the determination of the index of refraction of particles suspended in the ocean., J. Opt. Soc. Am., 63 : 321

Zaneveld, J. R. V., Roach, D.M., and Pak, H., 1974, The determination of the index of refraction distribution of oceanic particulates., J. Geophys. Rs., 79 : 4091

APPENDICES

APPENDIX I

Effect of Water-Glass-Air Interfaces on Scattering Angle

Because of the differences in indices of refraction between water, glass, and air, light that is scattered at some angle, θ, from the collimated beam in water will no longer be traveling at angle θ after it passes throught the glass lens of the narrow angle scattering meter and into the air. Specifically, for this experiment, the theoretical path of a ray scattered at angle θ, in water, is shown in Figure 30. By choosing a ray that passes through the center of the lens on the glass-air interface, the solution of the problem is simplified.

From Snell's law:

$$\frac{\sin \theta}{\sin r_1} = \frac{n_{glass}}{n_{water}}$$

and

$$\frac{\sin r_1}{\sin r_2} = \frac{n_{air}}{n_{glass}}$$

$$r_2 = \sin^{-1}\left\{\frac{n_{water}}{n_{air}} \sin \theta\right\}$$

$$x = \tan r_2$$

$$x = \tan \{\sin^{-1}(1.33 \sin \theta)\}$$

where x is in meters.

This computation provides a means of correlating detector platform movement (i.e. X-axis on the X-Y recorder) with actual scattering angle. One millimeter of platform movement corresponds to 28.4 millimeters of X-axis movement. Table 10 shows the calibration of platform position, X-axis position and actual scattering angle, θ.

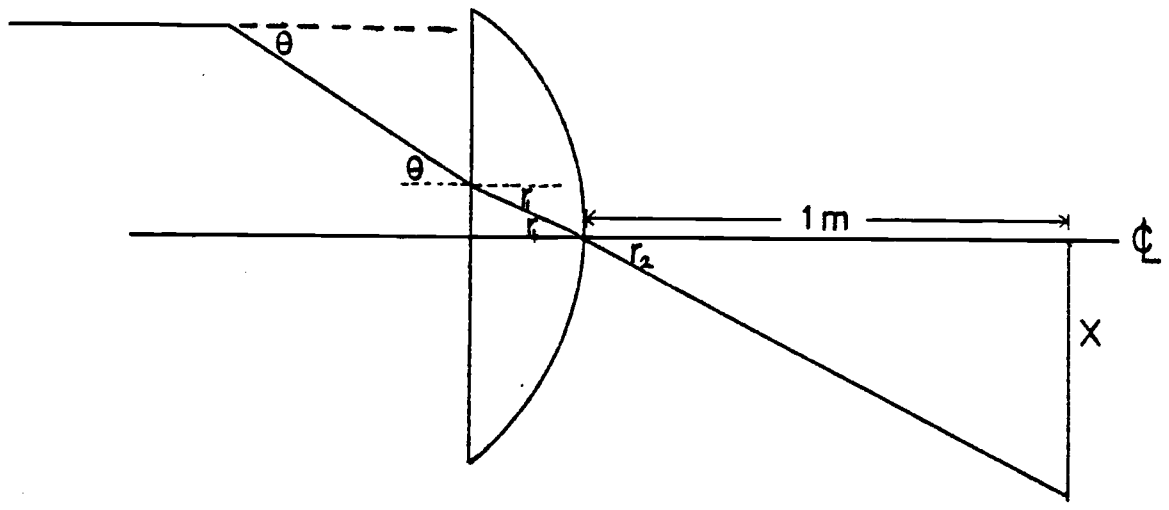

Fig. 30 Effect of water-glass-air interface on scattering angle, θ.

Table 10

CALIBRATION OF DETECTOR PLATFORM POSITION, RECORDER X-AXIS POSITION, AND ACTUAL SCATTERING ANGLE, θ

Scattering Angle, θ	Platform position	X-Axis position
0°	0 mm	0 mm
0.1°	2.76 mm	66.04 mm
0.15°	3.48 mm	99.06 mm
0.2°	4.64 mm	132.08 mm
0.25°	5.80 mm	165.10 mm
0.3°	6.96 mm	198.12 mm
0.35°	8.12 mm	231.14 mm
0.4°	9.29 mm	264.16 mm
0.45°	10.44 mm	297.18 mm
0.5°	11.61 mm	363.22 mm
0.55°	12.76 mm	363.22 mm

APPENDIX II

FOCAL Computer Programs

I. Calculation of theoretical volume scattering function

```
1.10   S BETA=Ø
1.12   S CT=Ø
1.20   A ?THETA?
1.30   F I=1, 17; A N(I)
1.40   T !!
1.45   0 R
1.50   F J=1, 17; A S(J)
1.60   T !!
1.70   F K=1,17; D 1.71
1.71   S BETA=BETA + N(K)*S(K)*5.072E-9
1.72   S CT=CT + 1
1.74   IF (CT-4) 1.30, 1.80, 1.80
1.75   S BETA=BETA/240
1.80   T %, "AT THETA",THETA, !, "THE THEORETICAL SCATTERING IS"
1.81   T %, BETA, !
1.90   QUIT
```

Sixty eight values of the number of particles in each of sixty eight size ranges determined by the particle size analyzer are punched in by the user on the keyboard (first two values are always zero). This is done in four groups of seventeen. After each group of seventeen is punched the high-speed reader reads a tape containing scattering values for single particles in each size range at a particular angle. This program has been run for values of θ of 0°, 0.2°, 0.5° and 1°.

II. Calculation of experimental volume scattering function

```
1.05   ASK  ?X?, !
1.10   F I=1, 10; A P2(I)
1.20   T !
1.30   F J=1, 10; A P1(J)
1.40   D 1.20
1.50   F K-1, 10;S BETA(K)=(P2(K)-P1(K))|((X-1)*(1.25E-7*3.1416))
1.60   S THETA=.1
1.70   T !, "    THETA    BETA(THETA)",!
1.72   S L=1
1.80   T %, THETA,"      ", BETA(L), !
1.90   S L=L+1; S THETA=THETA +.05
2.10   IF (L-10) 1.80, 1.80, 2.20
2.20   T "THESE VALUES ARE FOR A CONCENTRATION FACTOR", X, !
2.30   A ?PARTICLESIZE?
```

The term, X, is the concentration factor used (in this experiment X = 2). The ten values of P2 are the ten values of $\frac{P(\theta)}{P(o)}$ obtained for the higher concentration sample at θ = 0.1°, 0.15°, 0.2°, 0.25°, 0.3°, 0.35°, 0.4°, 0.45°, 0.5°, 0.55°. Similarly, the values of P1 are the values of $\frac{P(\theta)}{P(o)}$ obtained for the lower concentration sample, at the same angles.